Powder Technology 283 (2015) 415–432

Contents lists available at ScienceDirect

Powder Technology

journal homepage: www.elsevier.com/locate/powtec

Feedback control strategies for a continuous industrial fluidized-bed granulation process

Ivana M. Cotabarren *, Diego E. Bertín, Verónica Bucalá, Juliana Piña

Department of Chemical Engineering, PLAPIQUI, Universidad Nacional del Sur, CONICET, Camino La Carrindanga Km. 7, 8000 Bahía Blanca, Argentina

ARTICLE INFO

Article history:
Received 31 December 2014
Received in revised form 11 April 2015
Accepted 1 June 2015
Available online 9 June 2015

Keywords:
Process control
Granulation circuits
Flowsheet simulation
Population balance model
Solid processes
Urea fertilizer

ABSTRACT

This paper focuses on enhancing the operation of industrial granulation circuits via the design and performance evaluation of different control strategies. Particularly, the control strategies were implemented on a urea flowsheet simulator based on the Uhde fluidized-bed granulation technology (UFT), previously developed in the gPROMS modeling environment (Process System Enterprise) and validated against experimental data by our research group. First of all, an effective strategy for variable pairing in MIMO systems through Relative Gain Array analysis was tested. Continuing with the control system design, the controller parameter tuning was performed coupling an integral of time absolute error method with an optimization strategy. Afterward, the ability of single-loop feedback controllers (PI) to reject operational disturbances and track desired set-points was analyzed. Multiple-loop feedback strategies, such as cascade control were also implemented to improve controller performance. All the studied control loops were effective to either eliminate disturbances in the granulation circuit variables or to reach new set-points for the controlled variables, although it is demonstrated that the cascade configuration outperforms the single-loop feedback control strategy. Summarizing, this contribution provides granulation process engineers with useful control strategies for solving typical transient operational challenges.

1. Introduction

Within particle technologies, granulation is a fundamental operation of widespread use. It converts fine particles and/or atomizable liquids (suspensions, solutions or melts) into granular material with desired properties [1]. Typically, three components are needed to produce granules: initial seeds or nuclei, mixing and a binder. The seeds are always agitated to achieve a good distribution of the binder. Depending on the mixing principle, granulators are often classified into mechanical (e.g., pan, drum, high shear granulators) or pneumatic (fluidized-bed granulators) agitated units [1]. Fluidized-bed granulators (FBGs) offer some advantages, with respect to other granulation systems, since they allow us to integrate spraying, size enlargement, drying and/or cooling stages in one single unit [2–4].

Granulation processes are usually also classified according to the binder nature as wet, dry or melt. In wet granulation, the liquid binder (a solution or dispersion) is distributed on the seeds and, subsequently, the granules are dried to evaporate the solvent. In dry granulation, fine solid particles are added to the agitated seed bed; the powder adherence is promoted by Van der Waals or electrostatic forces [5]. In melt granulation, powders are enlarged by using meltable materials. These last binders are added to the systems either as powders that melt during the granulation process or as atomized molten liquids [6].

In general, not all the particles that leave the granulation unit meet the marketable granule size distributions, being necessary other unit operations such as crushing and size classification. The combination of all the involved process units (i.e., granulator, crusher, screens, etc.) constitutes the granulation circuit [7]. The operation of granulation circuits is not simple and often presents operational challenges, which force them to work with a capacity less than the nominal one and with high recycle ratios that overload all the process units [8,9]. Furthermore, the design and operation of these circuits are often performed by trial and error and based on previous experiences [4]. To mitigate this situation, it becomes critical the design and control of granulation circuits under an integrated approach, aided by the progress in numerical techniques and computer resources [10]. It is widely accepted that for processes that handle liquid and gases the development of computing tools to simulate, optimize and control large-scale processes has been one of the most important engineering advancements. Nonetheless, many difficulties arise when process system engineering tools are intended to be applied to processes that handle solids due to their complex nature. While engineering processes involving fluids require relatively few variables to describe the system behavior completely (e.g. temperature, composition, pressure), solid process streams involved lumped variables as well as distributed properties (e.g. particle

* Corresponding author. Tel.: +54 291 486 1700x269; fax: +54 291 486 1600.
E-mail address: icotabarren@plapiqui.edu.ar (I.M. Cotabarren).

http://dx.doi.org/10.1016/j.powtec.2015.06.010
0032-5910/

size, porosity, moisture distributions) [11–13]. The mathematical representation of powders transformations is not a trivial task. One well-established framework for the macroscopic modeling, and well-suited for industrial-scale processes, is the population balance equation (PBE). This tool was first introduced in the field of statistical mechanics by Hulburt and Katz [14] and later applied to the field of particulate process, among many others, by Randolph and Larson [15], Hounslow et al. [16], Ramkrishna et al. [17], Peglow et al. [3] and Li et al. [18]. In fact, the population balance equation allows predicting the change of distributed selected particle properties (e.g., size) by different mechanisms, although it is commonly defined by a complex partial integro-differential equation [9,19].

Even though particulate processes are involved in approximately three quarters of all industrially processed goods [20] and despite their imperious necessity of controllability, the analysis and development of general control design methods remain a difficult task. This is due not only to the distributed nature of the PBE (i.e., infinite number of internal states) and the nonlinear and multivariable input–output behavior of such processes, but also to the lack of reliable sensors for the in-line monitoring of distributed properties (e.g., particle size, moisture, porosity), the insufficient degrees of freedom or manipulated variables, and the current batch or semibatch operation of many processes, especially in the pharmaceutical industry [19,21].

In the last few years, several attempts have been made towards the control of particulate processes. Probably, the greatest advances regarding the design of nonlinear controllers have been performed by Christofides' group at the University of California [22–29]. Specifically, their approach consisted in reducing the order of the PBE by different techniques (i.e., method of weight residuals combined with approximate inertial manifold or method of moments) to subsequently design robust nonlinear controllers with stable closed-loop responses and relatively low computational cost [22,25]. Afterwards, the design also incorporated uncertainty in model parameters and unmodeled actuator/sensor dynamics and constraints on the capacity of control actuators [23,24]. The proposed methods have been developed to control the particle size distribution (PSD) in batch and continuous crystallizers, aerosol and thermal spray processes.

Regarding wet granulation technology (in rotary drums, high shear mixers and pan granulators), where particles mainly grow by agglomeration, several control strategies have also been proposed. Particularly, Zhang et al. [30] implemented on a di-ammonium phosphate (DAP) drum granulation pilot plant a simple proportional–integral (PI) controller to control the oversize fraction of the recycle stream, by manipulating the water flowrate to the drum. Pottmann et al. [31] introduced Model Predictive Control (MPC) strategies to control the granule PSD (by tracking the particle diameters corresponding to 5 and 90% of the mass cumulative curve) and density by manipulation of the binder flowrate of a generic granulation circuit (presenting either a pan, rotary drum or high shear granulation unit with agglomeration as the main size enlargement mechanism). Gatzke and Doyle III [32] extended Pottmann et al. [31] study by the formulation of soft constraints and a prioritized control strategy to avoid unattainable set-points. By using a model validated against data from a laboratory-scale high-shear granulator, Sanders et al. [33] compared the use of a proportional–integral-derivative (PID) controller with a MPC strategy to control the granulation unit. As the model did not include the complete circuit, the manipulated and control variables were only related with the high-shear granulator operating conditions. Glaser et al. [34] developed a robust MPC control strategy for a drum continuous granulation plant. They used, for the different circuit units, models validated against experimental data from a pilot-scale plant to analyze the process controllability with the aim of extending it to the industrial scale. These authors considered either the fresh solid feed or the feed moisture to solid ratio as manipulated variables for controlling the mean size of the granulator product. Finally, Ramachandran and Chaudhury [10] extended Glaser et al. [34] study by considering a novel PBE formulation and implementing PI controllers to the multiple-input multiple-output drum granulator system.

Concerning continuous fluidized-bed granulators, Heinrich et al. [35,36], Drechsler et al. [37] and Radichkov et al. [38] studied circuits including this type of technology. In those systems, the corresponding FBG is constituted by one chamber where wet granulation processes occur (i.e., the binder agent is a liquid suspension). Besides, constant granulator mass holdup or hypothetical particle size distributions for the outlet crusher stream were assumed. Considering that the PSD can be measured, Palis and Kienle [39–41] studied the stabilization of unstable steady-states detected by Radichkov et al. [38] in the abovementioned FBG circuit applying H_∞-theory and discrepancy-based control. Finally, Bück et al. [20] applied a standard linear PI structure and a non-linear MPC to stabilize the operation of the fluidized-bed system studied by Heinrich and coworkers with internal and external product classification, respectively. For the PI controller, a linear transfer function relating the manipulated (suspension spraying rate) and controlled variable (PSD third moment, i.e. proportional to the total mass of particles in the bed) was derived after linearization of the mathematical model. The MPC controller manipulated the speed of the mill to control the average size of the milled particles by measuring the PSD second moment (i.e., proportional to the surface area of the particles exiting the mill), which required the PBE linearization around the steady-state (discretization with respect to the particle size by a finite volume method) and time discretization.

It is also worth to mention the recent advances in control of continuous pharmaceutical process performed by the Engineering Research Center of Rutgers University. In-silico closed feedback control has been tested in tablet manufacturing processes via direct compaction [42], roller compaction [43] and wet granulation [44] with advances in MPC implementation for the same configurations [45].

It is important to note that the granulation process is considered as one of the most significant developments in the fertilizer industry, providing products with higher resistance and lower tendency to caking and lump formation. In particular, granular urea is the most-consumed nitrogen-based fertilizer, being critical in the modern agriculture scenario [46]. Industrial urea granulation is mainly performed in fluidized-beds [7], which use a very concentrated urea solution as binder (basically molten urea) sprayed from the bottom. Due to the required industrial high production rates, high urea melt to seed mass ratios (about 50%) are employed. In the industrial practice, short granulation times are used and coating (i.e., layered growth) is the preferred size enlargement mechanism [9,47,48]. Unfortunately, and as granulation circuits in general, this process is usually operated by trial and error [49]. Among others, typical dynamic operational problems of the urea granulation circuits are: undesired plant shutdowns due to the formation of lumps in the granulation unit (which can be triggered by several causes, e.g. too-high operating temperatures and low fluidization air flowrate); and continuous oscillations of product quality due to the cycling nature of the granulation circuits and changes of the desired product mean size to meet particular market demands. Furthermore, as exposed in the literature review, control of continuous industrial fluidized-bed melt granulation processes has not received much attention. Consequently, this work focuses on the design and performance evaluation of different single-loop feedback control and cascade strategies implemented on a urea flowsheet simulator based on the Uhde fluidized-bed granulation technology (UFT), which was previously developed and validated against experimental data by our research group [13]. As well, it is the aim of this contribution to provide granulation process engineers with control strategies for solving typical operational challenges.

2. Simulation environment and mathematical models

Fig. 1 shows the operation units typically encountered in the UFT urea granulation process, which are: (1) a multichamber fluidized-bed granulator for the particle growth, (2) a cooling unit to diminish

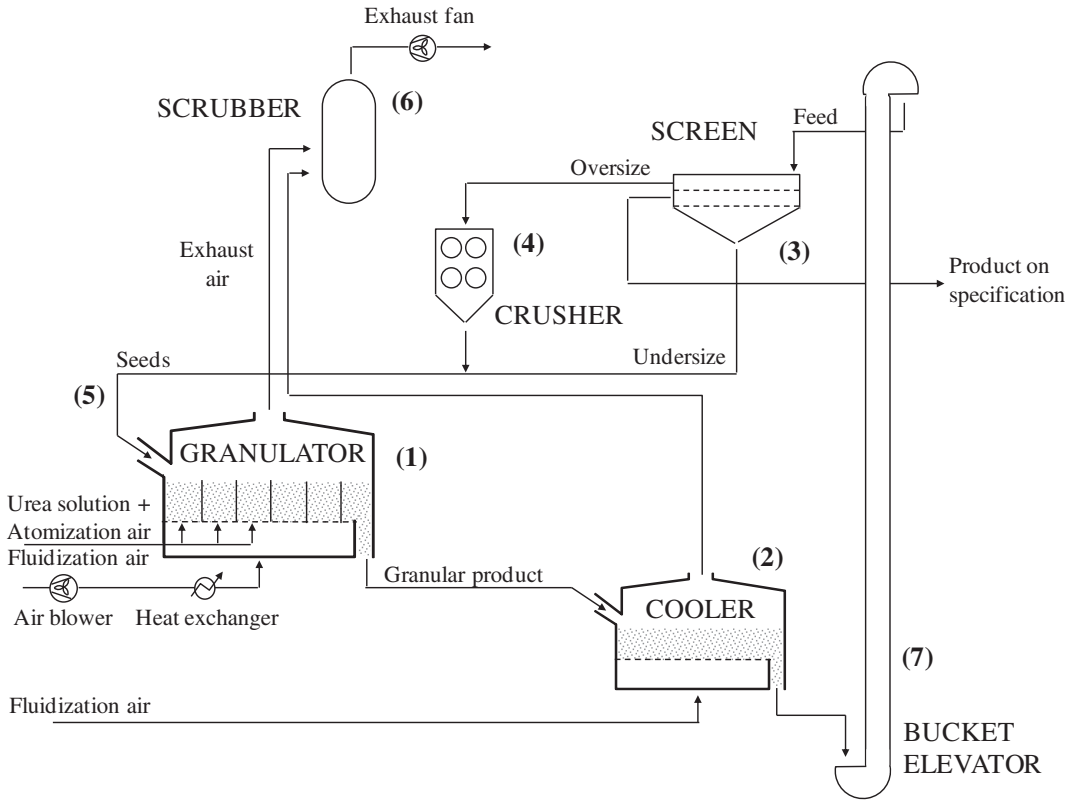

Fig. 1. Urea granulation circuit based on UFT fluidized-bed granulation technology. Adapted from [7].

the granule temperature and avoid undesirable lumps formation, (3) double-deck screens to separate the under and oversize particles from the marketable product, (4) double-roll crushers to grind the oversize material (therefore a recycle stream (5) containing the crushed oversize an the undersize streams is returned to the granulation chamber as seeds), (6) wet scrubbers for the exhaust air conditioning and (7) an elevator for material transportation [7].

In order to perform virtual experimentation, model validation and process optimization, extensive research has been undertaken to develop a flowsheet model to accurately represent the operation of an industrial urea granulation circuit (UGC). The details are reported elsewhere and briefly summarized here.

For the technology studied in this contribution, the granulation unit is constituted by several fluidized-beds. Typically, the first compartments are for granule growth while the last ones are reserved for particle conditioning and cooling. The seeds are constantly fed to the fluidized-bed granulator while a concentrated urea solution (usually called urea melt due its high urea concentration, which is about 96 wt.%) is sprayed from the bottom of the unit [50,51]. The particles grow by deposition of the concentrated solution drops onto their surface and the subsequent evaporation of the water content and solidification of the urea present in the droplets. The fluidization air is taken at atmospheric conditions by a single blower and later derived to each chamber by a series of dampers. The air that enters to the growth chambers can be preheated by heat exchangers, which allow regulating to a certain level the fluidization air temperature [47,48]. The granulator chamber's temperatures are not only determined by the sensible heats corresponding to the streams that enter and/or leave each chamber, but also by the latent heats associated to the urea solidification and water evaporation. As a result, the granulator growth chambers normally operate between 109 and 112 °C. Temperatures higher than 100 °C guarantee the solution water evaporation, while temperatures lower than 133 °C avoid undesired agglomerate formation by urea particle melting [47,48]. The last chambers operate between 70 and 90 °C because the particles are fluidized with air at ambient conditions and no urea solution at high temperature is atomized [47].

The chambers are delimited by separating weirs with openings at the bottom that allow particle underflow by the principle of communicated vessels [52]. The fluidized-bed levels within each chamber have to remain below the height of the separating weirs to ensure that no solids will overflow, and over a minimum recommended height to guarantee that no drops will be sprayed over the fluidized beds in the growth chambers [47,48]. The granulator product discharge is performed by ducts located at the bottom of the last chamber. These ducts present swing type valves that can be adjusted to regulate the solid discharge [50,53]. To favor dust extraction, the granulator top is maintained under a certain underpressure (usually between −0.004 and −0.0044 bar g [48,50]). Unlike previous contributions, in this work the granulator top pressure varies according the scrubber operation, which is modeled by the equations described in the appendix section. The granulator chambers operate as parallel systems, i.e. with the same total pressure drop. Therefore, against any change in the beds hold-ups, the fluidization air is automatically redistributed. The fluidized-bed granulator model has received extensive attention in previous contributions [13,54,55]. This model was developed considering coating as the main size enlargement mechanism and based on non-steady state mass, energy, momentum and population balances for all the granulator chambers. For the sake of clarity, the granulator model has been included in the appendix section.

After the particles leave the granulation unit, the product stream is fed to a fluidized-bed cooler. This unit operates as one of the granulator cooling chambers; therefore, the afore-described model was adapted to the particular design and operating features of the cooler, taking into account a urea solution injection equal to zero.

The circuit classification step is performed by double-deck vibrating screens situated downstream of the fluidized-bed cooler. The

mathematical model that represents the performance of this unit was developed in a previous contribution which includes validation against industrial data from a high capacity granulation plant. It allows predicting the PSD and flowrates of the all unit streams by determining each deck's oversize partition coefficient as a function of operating and design variables [56].

The particles classified as oversize by the screens are then fed to double-roll crushers with variable gaps (one between the upper pair of rolls, and one between the lower one) in order to reduce their sizes to be suitable as seeds for the granulator. The model for this unit was also previously developed and allows predicting the PSD of the fragmented particles as a function of the feed PSD and gap settings. The parameters corresponding to this model were, as well, fitted against industrial data [57].

The urea granulation circuit model, including each unit mathematical representation, was implemented under the gPROMS Model Builder Environment. This is a multipurpose tool, mainly used to build and validate process models, comprising steady-state and dynamic optimizations among several other functions [58]. Its flexibility and robustness has been widely proved by many other workers, including processes involving particulate solids such as antisolvent crystallization or continuous pharmaceutical manufacturing processes [21,42–44,59].

For this work, the urea granulation circuit simulator was implemented in a flowsheet type structure, easily accessible for users unfamiliar with advanced mathematical models (i.e., operator training). To this extent, gPROMS offers the possibility to create a library of models which can then be used in the construction of flowsheets by simple "drag & drop". Consequently, an individual library entity was generated for each of the granulation circuit operation units, based on the previously validated models. Afterward, material connection ports were created for each of the entities in order to transfer between them information regarding the streams' temperature, mass flowrate and PSD. Control ports were set as well to further connect the ad-hoc models with the developed controllers. In order to facilitate data input (i.e., process variables and parameters, material properties, equipment dimensions, initial conditions), specific dialog-boxes were created for each of the operation units. The flowsheet overall performance was studied in a previous contribution by verifying that the mass balances are satisfied throughout the process and that the particle residence time in each unit is correctly captured [60].

3. Control system design

This section includes a detailed procedure for the design of single-loop feedback controllers for the granular urea production by the UFT fluidized-bed technology. To this end, the built-in controller models available in the Process Model Library (PML) of gPROMS were connected to the previously developed plant integrated flowsheet.

3.1. Selection of controlled and manipulated variables

In general, multivariable systems involve multiple inputs (manipulated variables) and multiple outputs (controlled variables) to deal with multiple control objectives associated with a process unit or a plant. Even though the presence of a MIMO system makes more challenging the task of the control engineer, it may also offer opportunities for advanced control applications [61]. In fact, one of the key decisions in multivariable systems involves the structure of the control system; specifically, the pairing of the controlled variables with the manipulated variables.

As depicted in Fig. 2 through block diagrams for the main granulation circuit process units, the UGC clearly constitutes a MIMO system. Regarding the granulation unit, it is important to maintain between certain limits the chambers fluidized-bed levels (L_k), temperatures (T_k) and top underpressure (P_{top}). For this unit, the possible manipulated candidates are: the urea melt flowrate injected to the growth chambers

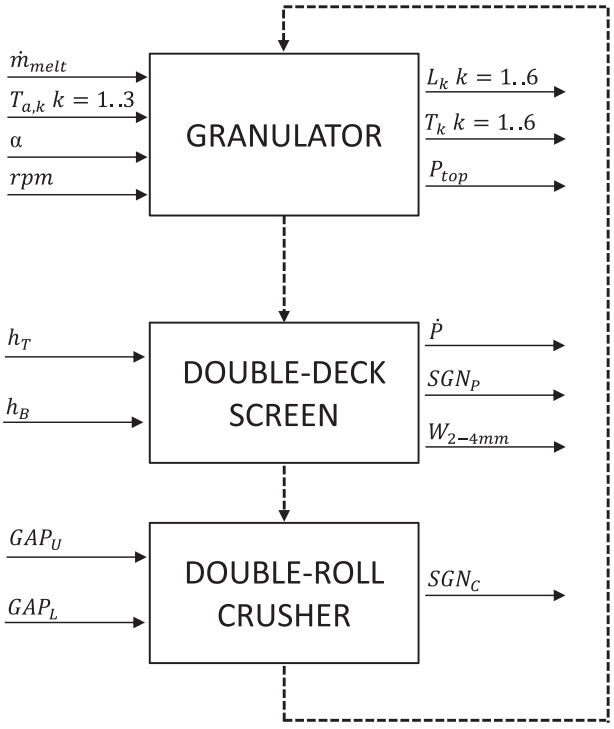

Fig. 2. Process block diagram.

($\dot{m}_{melt}$), the position of product-discharge duct swing-type valves (α), the temperature of the fluidization air entering each growth chamber ($T_{a,k}$) and the fluidization air blower revolutions per minute (rpm) (i.e., the total air fluidization flowrate). In the double-deck vibrating screens, the most critical variables to monitor are those related to the product stream (i.e., product mass flowrate ($\dot{P}$) and PSD). In the fertilizer industry, the PSD is usually characterized by the Size Guide Number (SGN_p), which is the mass median (i.e., granule size for which the passing cumulative mass percent fraction is equal to 50 wt.% value) of the particle size distribution multiplied by 100, and the mass fraction of particles between two selected sizes that is an indicative of the PSD width. For urea granules the desired size is close to 3 mm; therefore, the product mass fraction between 2 and 4 mm ($W_{2-4\ mm}$) is usually monitored [62]. For the screens, the variables most related to the product quality and process performance are the top and bottom decks' apertures (h_B and h_T). For the double-roll crusher, the possible actuator candidates are the spaces between rolls for both the upper and lower pairs (GAP_U and GAP_L) in order to regulate the milled PSD through its mean size (SGN_C).

It is important to note that between all the manipulated variable candidates, both deck effective apertures are not appropriate to control product quality as they cannot be freely manipulated during a normal continuous operation. In fact, although the circuit performance is highly affected by the top and bottom deck apertures (as demonstrated by the sensitivity analysis previously performed [13]), these constitute design variables that may behave as possible process disturbances due to changes by deck fouling or blinding and/or wire deformation caused by urea particles or dust. On the other hand, the connection streams between units and the recycle stream to the granulator (dashed lines in Fig. 2) suggest that changes introduced in a given manipulated variable may also affect controlled variables of other process units. Therefore, and considering that the crusher performance is mainly governed by the lower gap [13], GAP_L becomes an appropriate manipulated variable to control the product quality. Similarly and if possible, the urea melt flowrate should not be considered as a manipulated variable candidate since it directly affects the plant throughput ($\dot{P}$) (in steady-state operation and neglecting dust entrainment, the urea atomized into the

granulator is equal to the product flowrate). Besides, plant disturbances can enter through this variable as it directly depends on the production of the upstream ammonia plant. To summarize, Table 1 presents the proposed manipulated and controlled variables considered in this contribution for the complete UGC. It is worth to mention that the *SGN* of the granulator product is not directly controlled because the quality of the marketable product is given by the PSD of the product classified as on-size by the screens. Instead, the control of SGN_p allows us to track the PSD of product to be sold.

According to our previous studies, among all the granulator chambers, it is critical to control the second chamber temperature and fluidized-bed level since they are the closest to the established limits [7,53]. Therefore, the granulation unit constitutes a square MIMO system with equal number of manipulated and controlled variables (i.e., 3×3), being the challenge to pair them properly. As abovementioned, the most suitable manipulated variable for the product PSD is the GAP_L, while there is need to select between two possible control objectives (SGN_p or $W_{2-4\ mm}$). The following section describes the detailed procedure for the pairing of manipulated and controlled variables.

3.2. Controller structure

In this section we discuss the design of the UGC controllers that best suit the stated control problem. Particularly and as the granulation unit constitutes a MIMO system, pairings between potential manipulated and controlled variables should be made such that interactions within control-loops are minimized. In fact, and as demonstrated in previously performed sensitivity analyses [13,63], the granulator fluidized-bed levels, temperatures and top underpressure can be affected in a different extent either by the granulator discharge or fluidization air flowrate (i.e., blower rpm) disturbances.

The first step for a proper controller design is to quantify the extent of interactions in the given process. To this end, the relative gain array (RGA) can be used [10,42]. The RGA can be obtained from the gains of the plant transfer function matrix (TFM), i.e., the matrix that relates the Laplace transform of the output vector (vector of controlled variables) to that of the input vector (vector of manipulated variables) [61].

To construct the TFM, the process manipulated and controlled variables were first defined as deviation variables with respect to a selected steady state:

$$\hat{y}_1(t) = L_2(t) - L_2^0 \tag{1}$$

$$\hat{y}_2(t) = T_2(t) - T_2^0 \tag{2}$$

$$\hat{y}_3(t) = P_{top}(t) - P_{top}^0 \tag{3}$$

$$\hat{u}_1(t) = \alpha(t) - \alpha^0 \tag{4}$$

$$\hat{u}_2(t) = T_{a,2}(t) - T_{a,2}^0 \tag{5}$$

$$\hat{u}_3(t) = \mathrm{rpm}(t) - \mathrm{rpm}^0 \tag{6}$$

Table 1
Proposed manipulated and controlled variables.

Controlled variables	Proposed manipulated variables
• Second chamber level (L_2)	• Second chamber fluidization air temperature ($T_{a,2}$)
• Second chamber temperature (T_2)	• Granulator discharge (α)
• Granulator top pressure (P_{top})	• Blower rpm (rpm)
• Product SGN (SGN_p)	• Bottom crusher GAP (GAP_L)
• Product on specification ($W_{2-4\ mm}$)	

considering the following equation for each TFM element:

$$g_{i,j}(s) = \frac{\hat{y}_i(s)}{\hat{u}_j(s)}. \tag{7}$$

Therefore, the TFM ($GG(s)$) can be represented as:

$$Y(s) = G(s)U(s) \tag{8}$$

where $Y(s)$ and $U(s)$ are the vectors of controlled and manipulated deviation variables, respectively.

The RGA (Λ) is defined by the Hadamard product (i.e., element-by-element multiplication) between the inverse and the transpose of the gains matrix. That is:

$$\Lambda = K^{-1} \times K^T \tag{9}$$

with K equal to:

$$K = \begin{bmatrix} k_{1,1} & k_{1,2} & k_{1,3} \\ k_{2,1} & k_{2,2} & k_{2,3} \\ k_{3,1} & k_{3,2} & k_{3,3} \end{bmatrix}. \tag{10}$$

The process gains ($k_{i,j}$) are found by calculating the ratio of the change in the steady-state value of $y(t)$ to the change in the steady-state value of $u(t)$. For example, $k_{1,2}$ is determined as:

$$k_{1,2} = \frac{\hat{y}_1(t)}{\hat{u}_2(t)} = \frac{L_2(t) - L_2^0}{T_{a,2}(t) - T_{a,2}^0}. \tag{11}$$

As expected, the gains matrix is independent of *s* (static) and the *i*th loop of a process is considered to be interacting with the *j*th loop if the *i,j* element of Λ ($\lambda_{i,j}$) is nonzero. Furthermore, the control pairing between the outputs y_i and the inputs u_j should be selected such that the relative gains $\lambda_{i,j}$ are positive and as close as possible to unity [61].

In order to determine matrix *K*, different open-loop simulations were implemented by performing step changes of ± 2.5, ± 5 and $\pm 10\%$ in the proposed granulator manipulated variables (α, $T_{a,2}$, $T_{a,k}$ and rpm) and registering the corresponding deviation values (expressed as percentage) for the controlled variables (L_2, T_2 and P_{top}). Unsurprisingly, Fig. 3a, b and c shows that changes in the granulator discharge and the air blower rpm affect all the variables to be controlled. Regarding the fluidization air temperature, it has a direct impact on the second chamber's temperature. Furthermore, it is interesting to note that even if this is a typical non-linear process, Fig. 3 demonstrates that it can be considered quite linear around the nominal steady-state. Therefore, for the chosen steady-state and considering the manipulated step changes and responses in deviation variables, the granulation process gains matrix can be approximated as:

$$K_{5\%} = \begin{array}{c} \\ L_2 \\ T_2 \\ P_{top} \end{array} \begin{array}{c} \begin{array}{ccc} \alpha & T_{a,2} & \mathrm{rpm} \end{array} \\ \begin{bmatrix} -1.350 & 2.556.10^{-4} & 2.364.10^{-4} \\ -10.835 & 0.231 & -3.135.10^{-3} \\ -289.22 & 0.082 & -0.0860 \end{bmatrix} \end{array} \tag{12}$$

with the following RGA array:

$$\Lambda = \begin{array}{c} \\ L_2 \\ T_2 \\ P_{top} \end{array} \begin{array}{c} \begin{array}{ccc} \alpha & T_{a,2} & \mathrm{rpm} \end{array} \\ \begin{bmatrix} 0.630 & -0.011 & 0.381 \\ -1.55.10^{-4} & 1.013 & -0.013 \\ 0.370 & -2.74.10^{-4} & 0.632 \end{bmatrix} \end{array}. \tag{13}$$

Clearly, the least interacting system is obtained when coupling: a) the granulator discharge with the second chamber fluidized-bed level ($\lambda_{1,1} = 0.630$), b) the fluidization air temperature with the second chamber temperature ($\lambda_{2,2} = 1.013$) and c) the air blower rpm with the granulator top underpressure ($\lambda_{3,3} = 0.632$). Even though $\lambda_{1,1}$ and $\lambda_{3,3}$

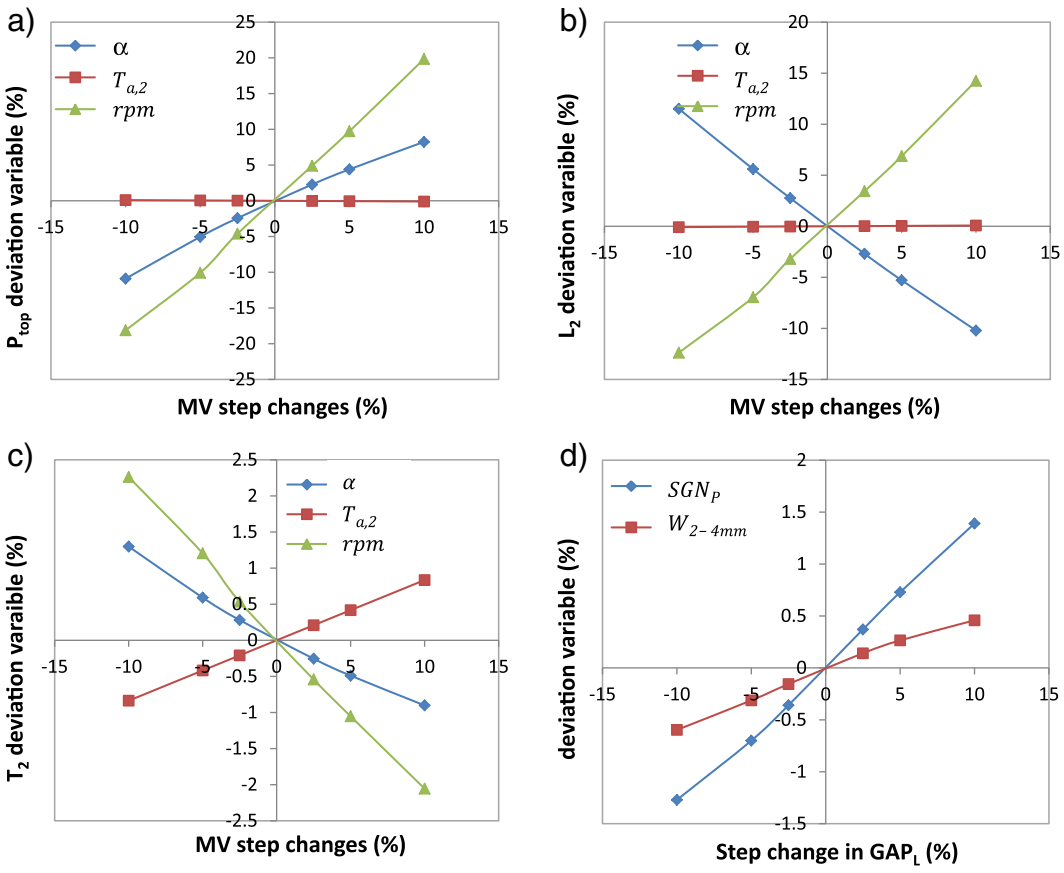

Fig. 3. Open-loop step responses.

are quite smaller than unity, they still represent acceptable values. However, interaction between these loops might be expected.

It is worth to mention that even if $K_{5\,\%}$ was determined for the responses obtained with a +5% step change in the manipulated variables, similar Λs were calculated for −5, ±2.5 and ±10% step changes (data not showed) due to the linearity of the process around the steady-state.

Regarding the control of product quality, as there is only one available manipulated variable (GAP_L) to control either SGN_P or the $W_{2-4\ mm}$, RGA analysis is meaningless and only open-loop step responses were evaluated to determine which presents more sensitivity to the crusher performance. Fig. 3d shows that the product *SGN* is more sensitive to changes in the bottom crusher gap than $W_{2-4\ mm}$ and therefore, more appropriate to be paired with GAP_L.

To summarize, Fig. 4 presents a screen-shoot of the UGC integrated flowsheet including the designed control structure. The manipulated and controlled variables associated to each loop are also indicated. It is important to mention that besides the main process units, the integrated flowsheet includes two grid converters (the crusher model was developed for a particle size grid different from that corresponding to the other models [57]) and two time delays to account for the particle residence time in the double-deck vibrating screen, the elevator and the double-roll crusher as well as possible instrumentation delays. Time delays 1 and 2 were arbitrarily established in 60 and 30 s, respectively. Even if the monitoring tools are not particularly modeled in this contribution, it is interesting to note that temperature, pressure and fluidized-bed level measurements can be performed using traditional liquid and gases industry sensors (e.g., thermocouples, pressure drop meters). In contrast, the in-line measurement of the average particle size of a stream (*SGN*) requires data acquisition methods suitable for particulate systems, which are usually associated with image analysis [4]. Some authors have extended theoretical control studies to batch laboratory scale systems using, for example, high-speed cameras that capture in-line images of the PSD [64,65]. Currently, other authors are evaluating its applicability to pilot scale [44]. Undoubtedly, the incorporation of this type of data acquisition systems incorporates delays that should be addressed by the implemented control systems. However, this contribution is based on in-silico implementation of the above control loops despising, in the first instance, delays associated to instrumentation data acquisition.

Finally, it is worth to mention that the initial steady-state selected in this contribution to perform the control studies corresponds to a stable open-loop operation.

3.3. Controller parameter tuning

Once the best variable pairing has been determined, it is necessary to tune the controllers' parameters. In this contribution, and due to their simplicity and widespread industrial use [66], all controllers are assumed to be proportional–integral (PI). Therefore, each controller is modeled by the following set of equations:

$$e_i(t) = y_i(t) - y_{SP_i}(t) \tag{14}$$

$$u_i(t) = K_{c_i}\left(e_i(t) + \frac{1}{\tau_i}\int_0^t e_i(t)dt\right) + bias_i \tag{15}$$

where $e_i(t)$ is the difference through time between the value taken by the controlled variable ($y_i(t)$) and the corresponding set-point value ($y_{SP_i}(t)$), $u_i(t)$ is the manipulated variable (i.e., controller output), K_{c_i} is the controller gain, τ_i is the controller integral time constant and $bias_i$ is the value of the manipulated variable when the error is zero. It should be noted that the error formulation varies if the control action is reverse (an increase in the manipulated variable generates a decrease

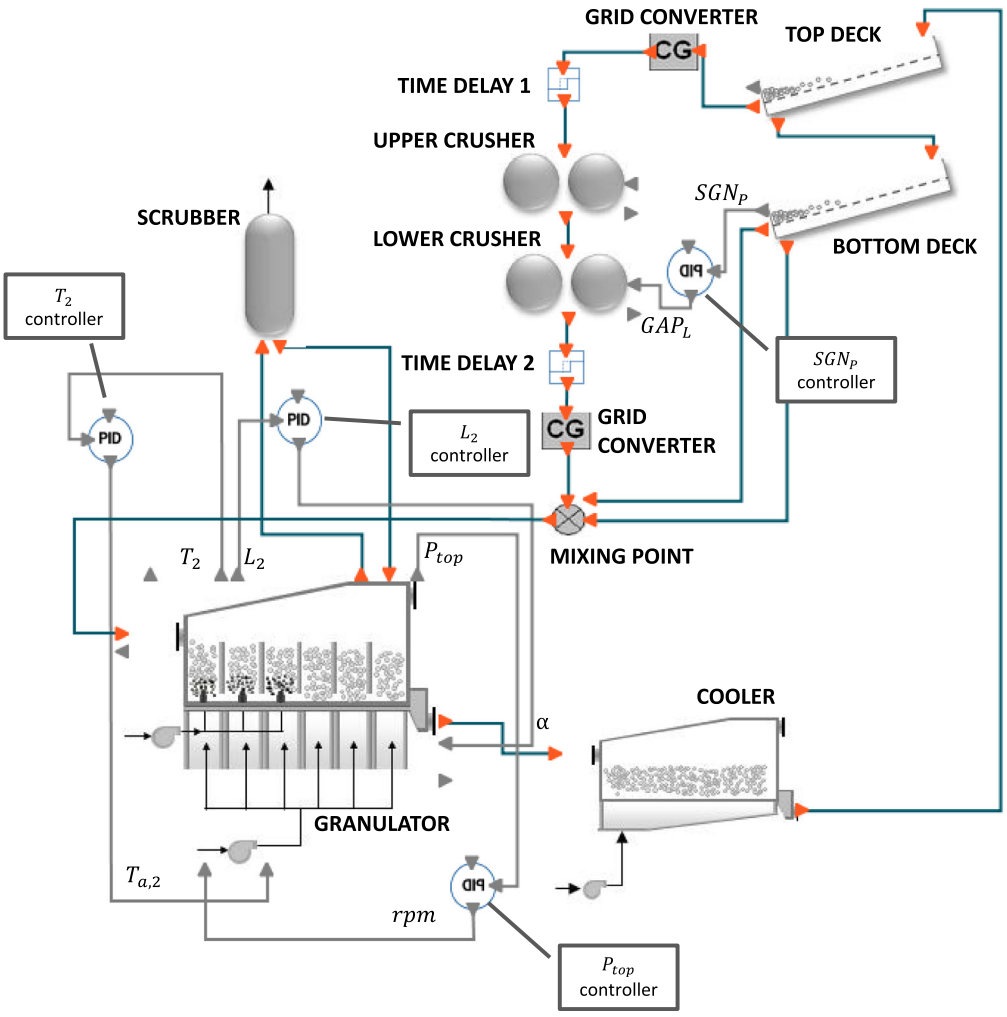

Fig. 4. UGC simulator flowsheet with integrated controllers.

in the process variable) or direct (an increase in the manipulated variable generates an increase in the process variable); in the latter case the error is formulated as $y_{SP_i} - y_i$.

As mentioned in Section 2, the UGC is implemented within the gPROMS flowsheet structure. Therefore, unit control ports are created to easily incorporate the PID model included in the PML control (Process Model Library Control) package. The controller model available in the gPROMS PML package allows the user to choose between several classes of controllers (P, PI, PIP, PD, I and D) and modes (manual, automatic and cascade). Furthermore, it is necessary to establish the maximum and minimum values for the manipulated (controller output) and controlled variables (input to the controller). As well, an anti-windup reset algorithm is included to ensure that the controller output lies within the specified upper and lower bounds. If the bounds are violated, the time derivative of the integral error is set to zero and once the controller output is back in the range of the bounds, the integral error changes according to the current error. The model also comprises scaling factors for the set-point, manipulated and controlled variables in order to improve the overall performance [58].

Considering that the present study involves four control loops (i.e., $i = 4$), it is necessary to determine eight control parameters (i.e., K_{c_i} and τ_i for each of the controllers). For this purpose, numerous methods and rules can be used. The most popular within the industry are heuristic methods such as Ziegler–Nichols (closed-loop tuning) and Cohen and Coon (open-loop tuning) and the methods based on the time integral of the error (i.e., ITAE, ISE, IAE) [61]. In this contribution, the controller parameters are adjusted using the ITAE (Integral of Time Absolute Error) criteria, which is often preferred since it gives more importance to errors that persist on time. To this end, a dynamic optimization is implemented in the gPROMS environment to minimize the following objective function:

$$\mathrm{OBJ} = \sum_{i=1}^{n} \left(\int_0^t t \; w \left| y_i(t) - y_{SP_i}(t) \right| dt \right) \tag{16}$$

where n is the number of control loops and w is a weight factor that allows avoiding scaling issues. The optimization is run for a time period long enough to achieve stabilization of the circuit variables. As suggested by Romagnoli and Palazoglu [61] for multi-loop tuning, a sequential procedure is followed. Firstly, each controller is tuned independently by the ITAE criterion, setting the other controllers in manual mode (Eq. (16) was formulated accordingly). Once a satisfactory performance is obtained for each loop, all the controllers are restored at automatic control and the tuning parameters are simultaneously refit using the individual results as the initial condition for the optimization problem. It is worth to mention that the optimization initial guesses for the independent tuning of the controllers were obtained by trial and error.

Table 2 presents the values of K_{c_i} and τ_i for each controller after solving the dynamic optimization, together with the rest of the parameters required by the gPROMS PID model. It is worth to mention that the ITAE

Table 2
Controllers' parameters.

Controller	K_c	τ	Min $u(t)$	Max $u(t)$	Min $y(t)$	Max $y(t)$	Bias	Control action
L_2	1.53E−3 [m^{-1}]	2.53 [s]	0	1.15	$0.06L_{weir}$	$1.2L_{weir}$	1	Reverse
T_2	10.29	5.92E−2 [s]	288 [K]	373 [K]	373 [K]	393 [K]	313 [K]	Direct
P_{top}	1.50 [rpm/Pa]	2.09 [s]	−140 [Δrpm]	140 [Δrpm]	98,000 [Pa]	101,325 [Pa]	0 [Δrpm]	Reverse
SGN_p	8.09E−4	1.57 [s]	GAP_L^{min} [mm]*	GAP_L^{max} [mm]*	200	400	GAP_L^0 [mm]*	Direct

* Absolute values cannot be reported due to confidentiality agreement.

value for each control loop is used as a performance criterion (i.e., the highest the ITAE, the worst is the controller performance).

4. Results and discussion

In this section, the performance of the implemented control-loops is evaluated. A well design controller needs to be able to reject plant disturbances as well as to track a desired set-point. Therefore, for guaranteeing robust performance, the sensitivity function $\varepsilon(s)$ should tend to zero (disturbance rejection) and the complementary sensitivity function $\eta(s)$ should tend to one (set-point tracking). In other words, there is a general constraint referred as [61]:

$$\varepsilon(s)+\eta(s)=1(SISO),\ \ \varepsilon(s)+\eta(s)=I\ (MIMO). \tag{17}$$

In the case of disturbances rejection, also referred as regulatory problem, the closed-loop performance is compared to the plant open-loop operation. For the set-point tracking, or servomechanisms problem, the controllers' performance is evaluated through the respective ITAE value. Finally, a more complex control structure performance is assayed by incorporating cascade controllers.

It is worth to mention that during the parameter adjustment, the optimizations were run every time with step changes implemented either in disturbance variables or in the control-loop set-point. Each set of controller parameters (the one obtained for set-point tracking and the one obtained for disturbance rejection) was tested for both types of problems, regulatory and servomechanism, and the one that resulted in best performance for either of them was finally selected. In this particular case, the controllers' performance was always superior with the set of parameters tuned for disturbance rejection (see Table 2).

Finally, it should be noted that in this contribution no measurement delays or noises are considered for the variables assumed as measurable.

4.1. Disturbance rejection

In first place, the ability of the control system to return the controlled variables to the nominal operation set-point values is tested. This was assayed by incorporating two types of disturbances: a) variations in the total melt flowrate injected to the granulator growth chambers and b) variations in the bottom deck screen opening due to typical wire fouling.

4.1.1. Urea melt flowrate disturbance

Regarding the urea melt flowrate, 5% step changes were introduced every 8 h (see Fig. 5a). Overall, the process was simulated in closed and open loop modes for 24 h. Fig. 5 shows the controlled variable time profile, presented as percentage of deviation variables $(y_i(t)-y_i^0)/y_i^0$. As it can be seen in Fig. 5b, the second chamber fluidized-bed level controller successfully returns the variable to the established set-point (note that the variable initial value coincides with the desired set-point). An increase in the injected urea melt incorporates more mass in each chamber; therefore, the fluidized-bed levels tend to augment as it is observed during the first hour. After this period, the manipulated variable effect becomes visible and the chamber's levels start to decrease until they stabilize in the desired value. Contrarily, the open-loop simulation presents an increasing profile, even surpassing the variable upper limit. On overall, the controller manages to return the controlled variable to its set-point value in approximately 4 h.

Regarding the top underpressure (Fig. 5c) and the second chamber temperature (Fig. 5d), both controllers perform very well, exhibiting a very fast response to urea melt increments. Although time delays of the measurement devices are expected in a real plant control implementation, it should be recalled that in this contribution the monitoring tools are not modeled and that the controlled and manipulated variables correspond to the same process unit (i.e., fluidized-bed granulator). As observed in Fig. 5c, the open-loop temperature response tends to increase the value against the assayed disturbances due to the higher thermal level associated to the injected melt. Concerning the granulator top pressure, increases in the urea melt flowrate affect the chamber fluidized-levels raising the corresponding pressure drop (see Fig. 5d). As a consequence, the momentum balance is modified and less fluidization air is fed to each chamber (data not showed). This reduces the underpressure created in the exhaust duct, as it can be inferred from the open-loop response.

The SGN_p controller (Fig. 5e) manages as well to return this variable to the desired set-point, although the response is quite sluggish. This is probably associated to the particle residence time in each unit, which delays the controller action. It also should be noted that, unlike the granulator controllers, this control loop relates controlled and manipulated variables corresponding to a different process unit; therefore, longer delays are expected. Despite this, the controller takes approximately 6 h to completely stabilize the SGN_p after the step changes are assayed (Fig. 5e) and the transient deviations are always lower than 1.3%. It is worth noting that the SGN_p is not significantly affected by urea melt flowrate disturbances, as previously verified [13]. Consequently, even in the open loop response, the SGN_p deviations with respect to the desired set-point are small. Fig. 5e also presents the time evolution of $W_{2-4\ mm}$ for the closed-loop operation. Although this variable is not controlled, it manages to maintain its value over the minimum required (i.e., 90% of the product mass).

Table 3 presents the ITAE value and standard deviation (SD) for each control-loop. Clearly, the top underpressure and temperature loops present the best performance with the lowest ITAE and small deviation values with respect to the desired set-points (0.0636 Pa and 0 K, respectively). Regarding the *SGN* and second chamber level control-loops, the ITAEs are higher, although the deviations with respect to the set-point values are quite low.

It is worth to note that all the variables present an oscillatory behavior, typical for systems with recycle streams. Nonetheless, it can be seen that the closed-loop simulation exhibit less oscillation than the corresponding open-loop. Hence, the implemented control structure improves the system stability.

4.1.2. Screen bottom deck fouling

In order to test the closed-loop simulator under typical operation problems, a reduction in the bottom-deck screen passage area was introduced as a process disturbance. The in-silico test was run by setting a linear diminution in the passage area due to wires' fouling (i.e., 10% reduction in the deck passage area after 10 days of operation, i.e. a fouling rate of 1%/day). This problem can arise, for example, when the urea dust generated during operation adheres to the screen wires enlarging their

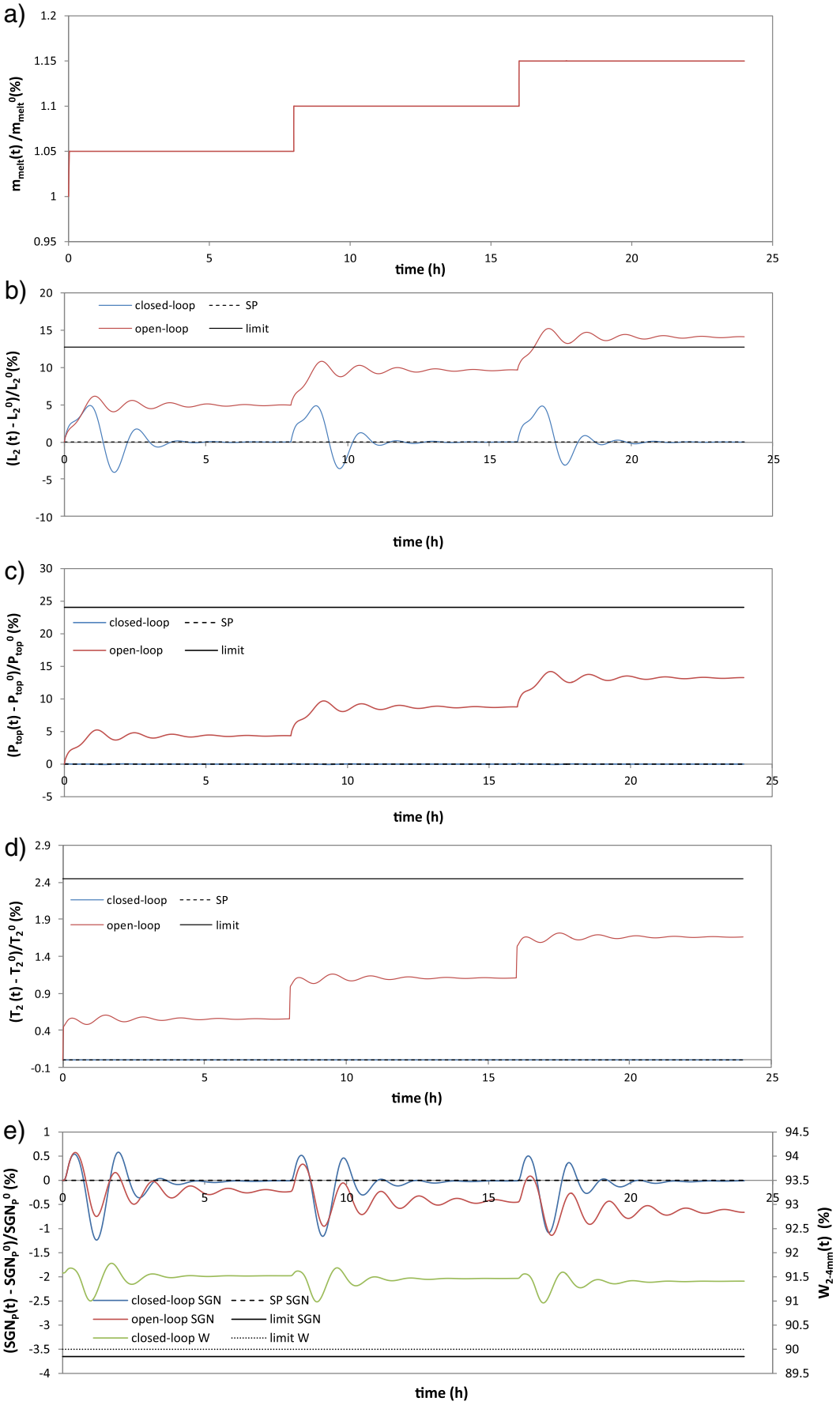

Fig. 5. Closed-loop performance for disturbance rejection (step changes in urea melt flowrate).

Table 3
Closed-loop disturbance rejection performance parameters (step changes in urea melt flowrate).

Controller	ITAE	SD
L_2	2.397E7 [m.s]	0.0222 [m]
T_2	6.223 [K.s]	0 [K]
P_{top}	897.011 [Pa.s]	0.0636 [Pa]
SGN_p	4.814E6 [s]	0.941 [–]

diameters. Even if this is a theoretical experiment, it gives insight to the closed-loop response under a particular operating challenge.

Fig. 6 presents the variable response in open and closed-loop modes. Clearly, as the assayed disturbance (Fig. 6a) presents a linear variation, all variables evolve linearly under open-loop operation. As observed, all controlled variables remain in the desired set-point value for the closed-loop simulation. Hence, the four implemented controllers manage to reject this type of disturbance successfully. Furthermore, it should be taken into account that the immediate response exhibited by the controlled variables (i.e., no visible time delay) is due to the small and progressively assayed disturbance (1%/day fouling rate). Essentially, when the bottom-deck passage area diminishes, fewer particles are classified as fines reducing the seed fed back to the granulator. This lowers the quantity of particles in each chamber and the corresponding fluidized-bed levels (open-loop mode in Fig. 6b). In order to maintain L_2 in the set-point value, the granulator discharge valve α needs to close, as observed also in Fig. 6b. A lower amount of particles in each chamber also modifies the momentum energy balance, which compensates the lower bed pressure drop with a higher fluidization air flowrate. As it can be seen in Fig. 6c for the open-loop simulation, this increases the

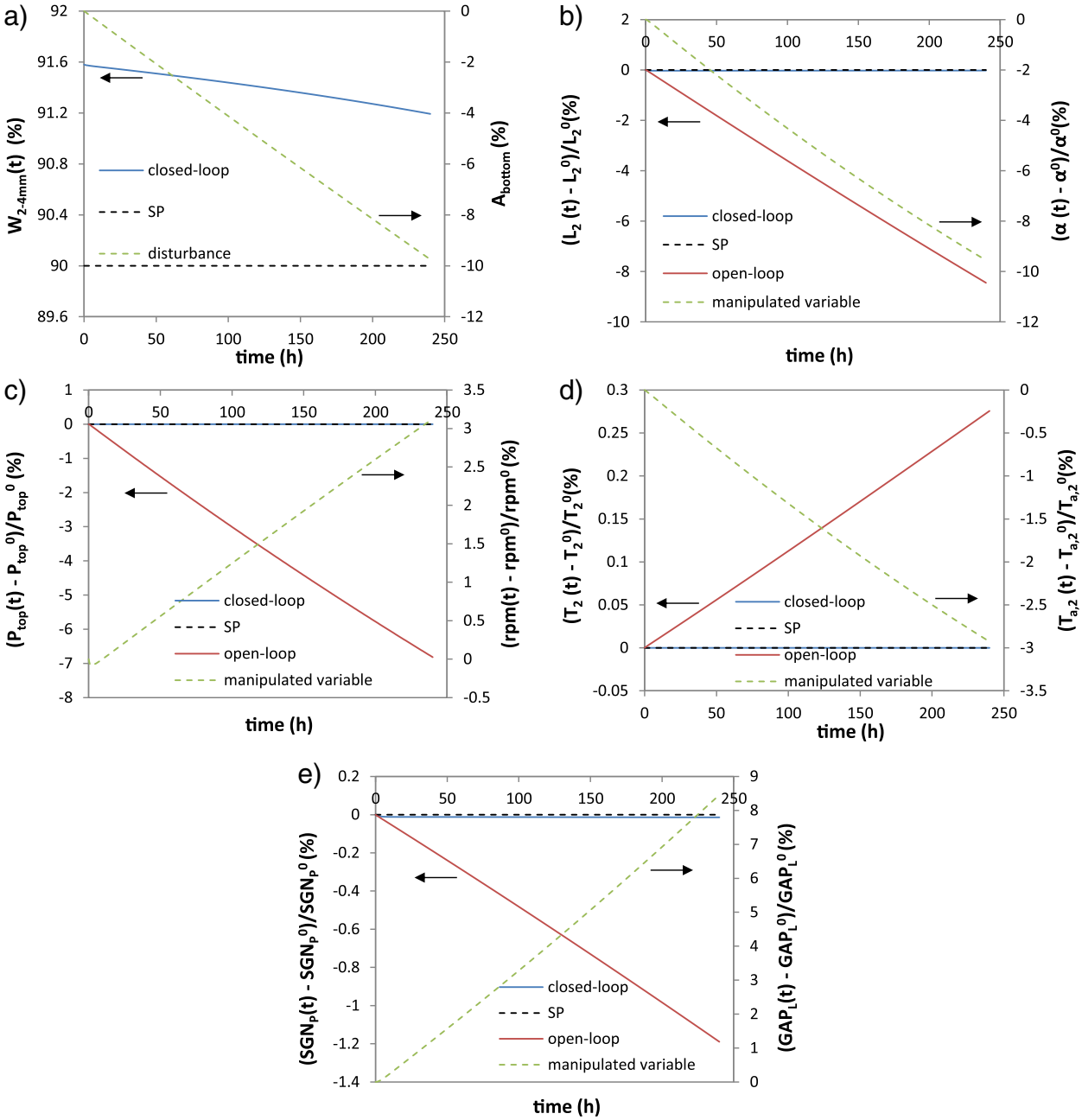

Fig. 6. Closed-loop performance for disturbance rejection (bottom-deck screen fouling).

granulator top underpressure. In order to return the controlled variable to the desired set point and provide the necessary fluidization air, the air blower operates at higher revolutions per minute. On the other hand, since each chamber is filled with a lower amount of mass, their temperature raises (open-loop mode in Fig. 6d) and the fluidization air temperature $T_{a,2}$ needs to be lower in order to keep the set-point value. Lastly, as the bottom deck aperture gets smaller, more fines are allowed to remain in the product stream lowering the SGN_p (Fig. 6e for open-loop operation). Consequently, the bottom gap increases its value to maintain the product specification. Regarding $W_{2-4\ mm}$, Fig. 6a shows that the assayed disturbance worsens this product quality variable, although during the simulated time it remains over the minimum allowable value. On overall, the performance in closed-loop is reasonable and feasible in real plant operation.

4.2. Set-point tracking

The ability of the implemented control structure to follow new desired set-points was also tested. All the controllers' set-points were modified during a complete plant simulation. The following profile was assayed: 1) at initial time, the T_2 set-point was lowered in 4 °C; 2) 8 h later, the set-point in SGN_p was modified from 280 to 290; 3) at

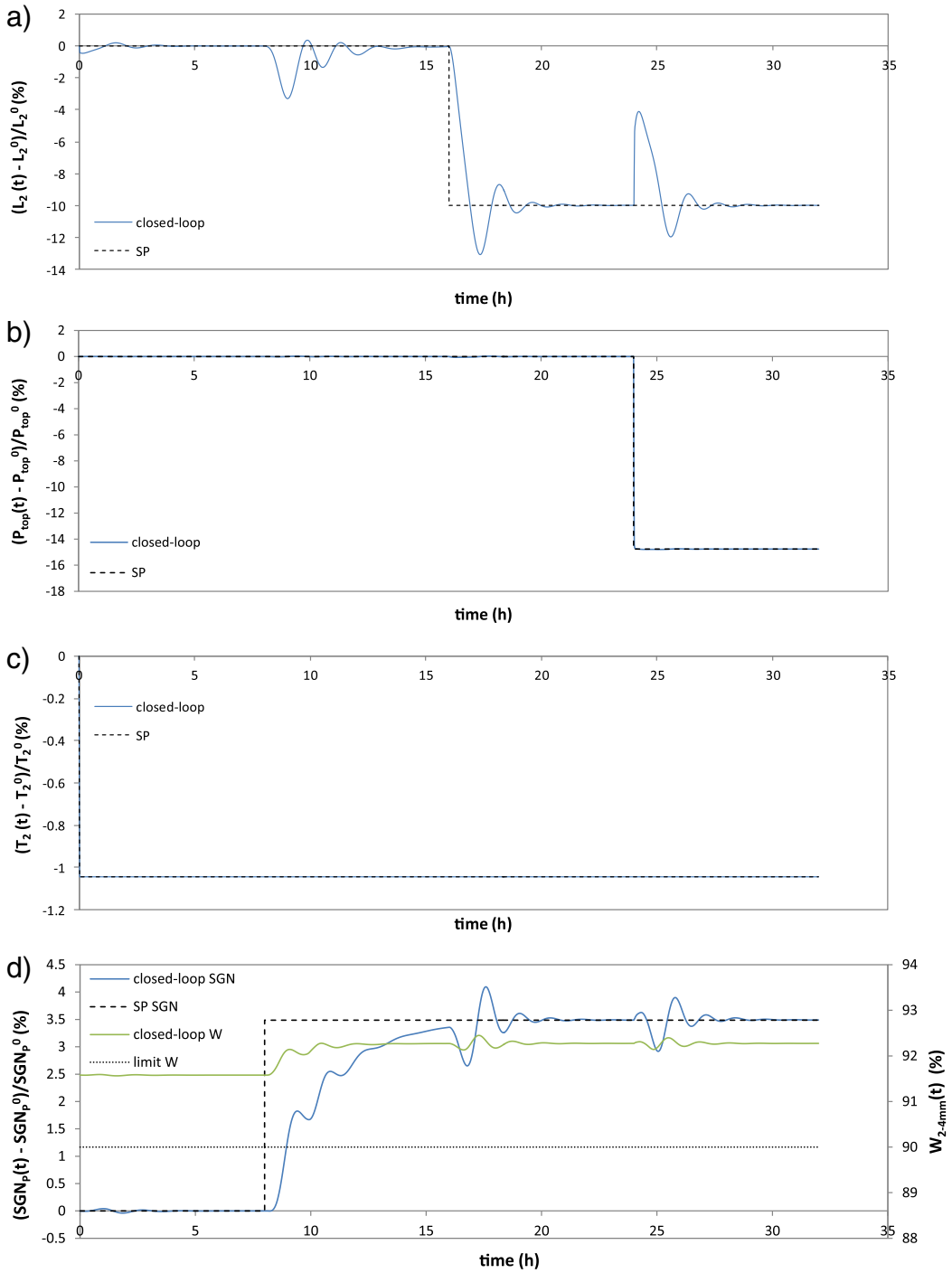

Fig. 7. Closed-loop performance for set-point tracking.

Table 4
Closed-loop set-point tracking performance parameters.

Controller	ITAE
L_2	4.250E7 [m.s]
T_2	5.7185 [K.s]
P_{top}	2313.95 [Pa.s]
SGN_p	1.591E7 [s]

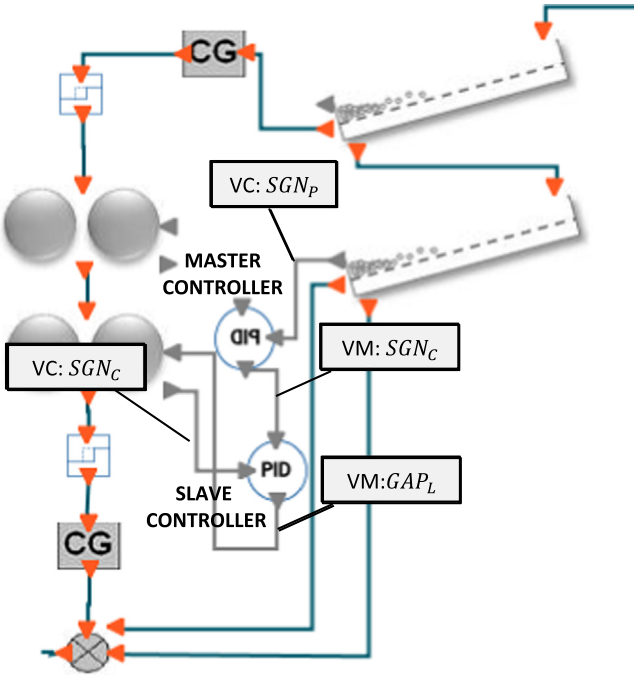

Fig. 8. Cascade control structure.

16 h, the second chamber level set-point was decreased a 10%; and 4) at 24 h, the granulator underpressure was modified in −15%.

Fig. 7 presents the closed-loop controlled variable time profiles. As for disturbance rejection, it is verified that the pressure and temperature control loops perform very well (Fig. 7b and c). In fact, and as it is reported in Table 4, low ITAE values are achieved. Regarding the second chamber level control-loop, Fig. 7a shows that the controller manages to reach the new set-point in an acceptable time taking into account the several delay times of the whole circuit, although this variable is also affected by changes in the SGN_p and P_{top} set-points (see Fig. 7). Both changes act as disturbances for the level controller as they modify in a certain extent the recycle flowrate to the granulator and the fluidization air flowrate. This controller presents the highest ITAE value. The pressure and temperature control loops are affected as well by changes of the second chamber fluidized-bed level and product SGN set-points. Nevertheless, as they quickly return to the desired values, the variation is not noticeable. Finally, the SGN_p controller is able to reach the new set-point, but once again exhibiting a sluggish response. Regarding $W_{2-4\ mm}$, Fig. 7d shows that although this variable is not controlled, it evolves to a new value higher than the admissible lower limit. L_2 and P_{top} set-point changes also act as disturbances for the SGN_p, being well rejected by the control-loop. The ITAE value related to this control is also given in Table 4.

Overall, even though the performance of all the developed controllers is acceptable either for servomechanism or regulatory problems, it is interesting to improve the time response for the SGN_p controller. This could be achieved by implementing a cascade control structure within this control-loop, as it is demonstrated in the following section.

4.3. Cascade control structure

A clear disadvantage of single-loop feedback control is that the controller action does not begin until the disturbance modifies the controlled variable. To avoid this, multiple feedback controllers can be associated in a cascade structure. This alternative improves the dynamic response by incorporating a second measurement variable (associated with a second control-loop) that recognizes the disturbances sooner than the controlled variable [67]. In connection to this, it is clear that the first stream that is affected by the manipulation of GAP_L is the crusher outlet. Therefore, SGN_C appears as an appropriate variable to detect, a priori, changes in the crusher operation. In this structure, the control-loop that measures the primary controlled variable (i.e. SGN_p) is called the master control-loop, which uses the set-point provided by the process operator. Accordingly, the loop that measures the second variable (i.e. SGN_C) is called the slave control-loop and uses the output of the master loop as its set-point to manipulate GAP_L. Details of the new control structure for SGN_p can be seen in Fig. 8.

Taking into account the afore-mentioned cascade control, the control structure presented in this section involves five PI controllers (i.e., three PI for L_2, T_2 and P_{top} and two controllers in cascade for SGN_p). The controllers' parameters were refitted following the previously described ITAE criterion and a new dynamic optimization was performed (the new controller parameters are presented in Table 5). As tested for the conventional structure, the closed-loop performance including the cascade controller was evaluated for both disturbance rejection and set-point tracking scenarios.

4.3.1. Disturbance rejection

The ability of the proposed control structure to maintain the desired set-points was tested by simulating the integrated flowsheet under the previously described profile in the urea melt flowrate (5% increments every 8 h, see Fig. 5a). Fig. 9 presents the closed-loop evolution of L_2 and SGN_p for the assayed disturbances with single-loop feedback controllers and cascade control. The second chamber temperature and the top underpressure time profiles were not included since it was clearly demonstrated in Sections 4.1 and 4.2 that these variables were successfully controlled. Fig. 9a shows that with the implementation of the cascade structure, the SGN_p returns faster and with less oscillation to the desired set-point than with the traditional single-loop controllers. In fact, the ITAE value for the master loop is almost 25% smaller than the ITAE presented with the traditional control configuration. Even if the

Table 5
Controllers' parameters for cascade configuration.

Controller	K_c	τ	Min $u(t)$	Max $u(t)$	Min $y(t)$	Max $y(t)$	Bias	Control action
L_2	2.01E−3 [m^{-1}]	4.10 [s]	0	1.15	$0.06L_{weir}$	$1.2L_{weir}$	1	Reverse
T_2	19.27	3.96E−3 [s]	288 [K]	373 [K]	373 [K]	393 [K]	313 [K]	Direct
P_{top}	3.89 [rpm/Pa]	9.10E−2 [s]	−140 [Δrpm]	140 [Δrpm]	98,000 [Pa]	101,325 [Pa]	0 [Δrpm]	Reverse
Master SGN_p	1.14E−3	1.65 [s]	50	300	200	400	280.23	Direct
Slave SGN_p	6.44E−4	0.95 [s]	GAP_L^{min} [mm][a]	GAP_L^{max} [mm][a]	50	300	GAP_L^0 [mm][a]	Direct

[a] Absolute values cannot be reported due to confidentiality agreement.

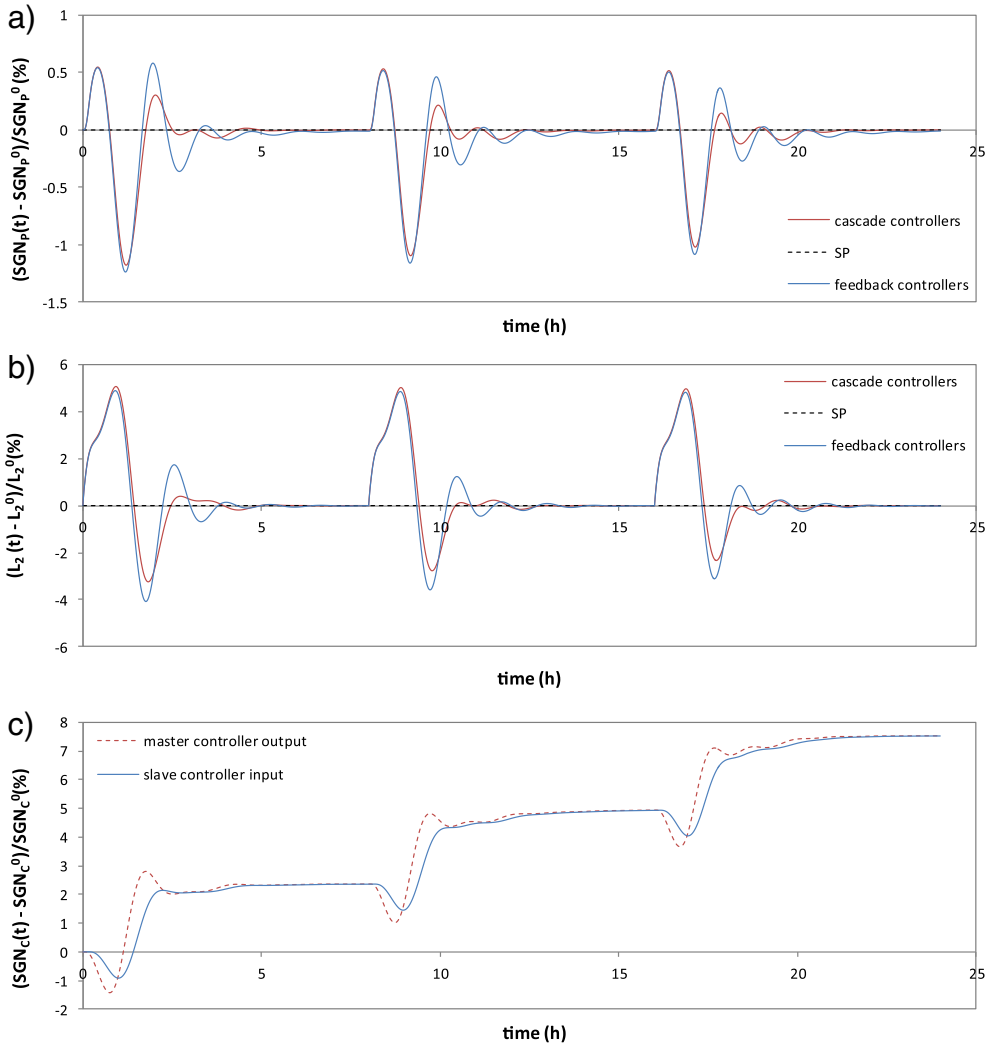

Fig. 9. Closed-loop performance for disturbance rejection including a cascade controller.

cascade structure is not directly applied to the fluidized-bed level controller, this variable also improves its performance as it is seen in Fig. 9b. The ITAE value in this case is almost 10% smaller than the previously obtained. Table 6 summarizes the ITAE and SD values for this analysis, including those corresponding to the temperature and underpressure control-loops. Compared with Table 4, all the ITAE and SD values are smaller. It is also interesting to test the ability of the cascade controller to reach the set-point for the additional measured variable (SGN_C). Fig. 9c shows that the slave controller input (SGN_C, controlled variable) reaches the corresponding set-point value within a delay period lower than 20 min, which is determined by the output of the master controller.

4.3.2. Set-point tracking

The closed-loop set-point tracking capacity was evaluated by incorporating the previously described disturbances (refer to Section 4.2). As well as for the regulatory problem, the evolution of SGN_p and L_2 for the assayed disturbances with single-loop controllers and cascade control was studied. Fig. 10a shows that this configuration is clearly more effective to drive the process to a desired new set-point in SGN_p. Disturbances corresponding to changes in other set-points are also successfully rejected. In fact, the ITAE for the master controller is reduced in 35% with the cascade configuration. For the second chamber fluidized-bed level, Fig. 10b shows that the variable slightly improves its performance when the change in L_2 set-point is assayed. However, for the set-point change in SGN_p (which act as a disturbance for this control-loop) the variable with cascade control presents less oscillations but with slightly higher amplitude than the single-loop controller structure. Overall, the ITAE value for L_2 increases by 2% considering the cascade configuration. Regarding the evolution of SGN_C, Fig. 10c shows that the set-point calculated by the master controller is satisfactorily reached by the slave controller. Table 7 summarizes the ITAE values for all the studied control-loops. It can be seen that, except for the chamber level control-loop, all the values are smaller than the ones presented in Table 4 (set-point tracking with single-loop controllers).

Table 6
Closed-loop disturbance rejection performance parameters including a cascade controller.

Controller	ITAE	SD
L_2	2.167E7 [m.s]	0.0213 [m]
T_2	0.189 [K.s]	0 [K]
P_{top}	11.647 [Pa.s]	0.0018 [Pa]
Master SGN_p	3.629E6 [s]	0.860 [–]

5. Conclusions

This work focuses on the design and performance evaluation of different single-loop feedback control and cascade strategies implemented

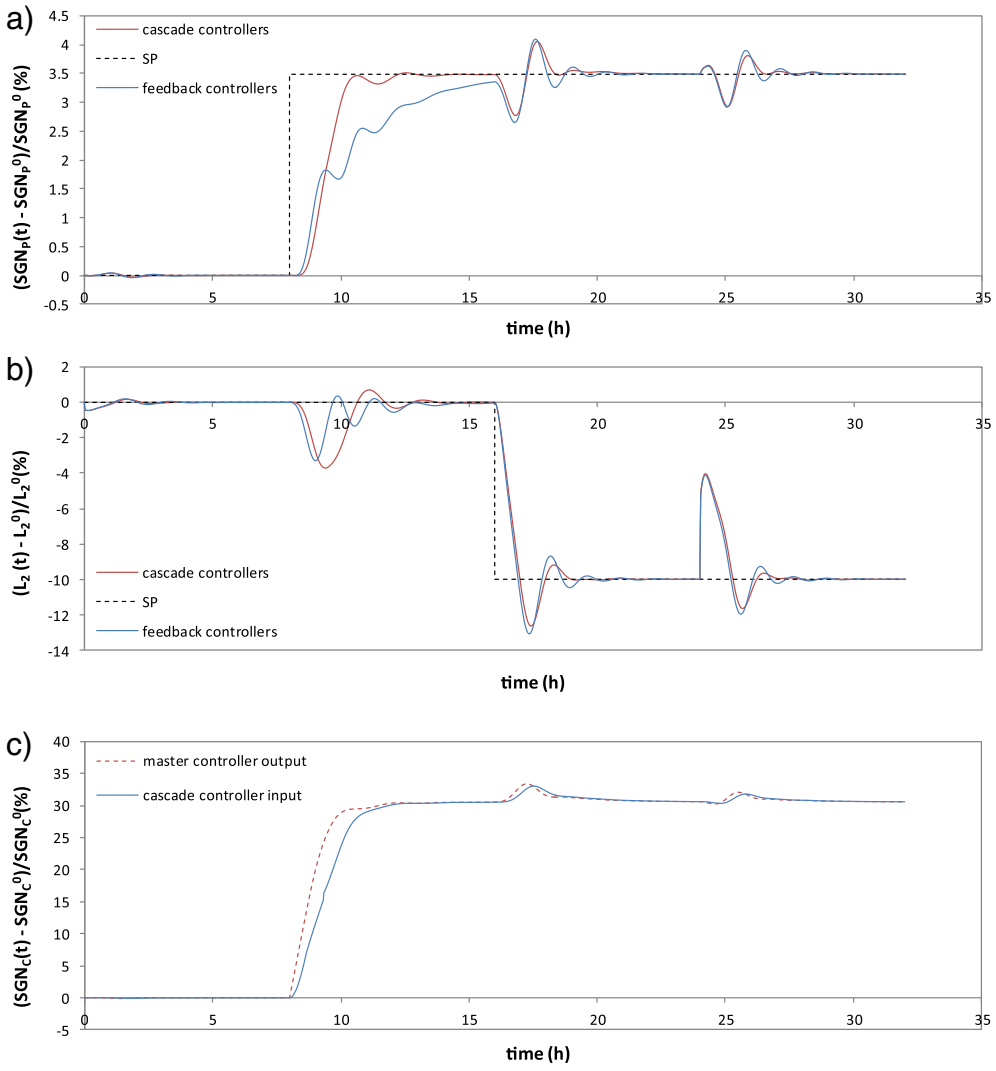

Fig. 10. Closed-loop performance for set-point tracking including a cascade controller.

on a urea flowsheet simulator (corresponding to a circuit based on UFT technology).

Within the potential circuit manipulated and controlled variables, process knowledge allowed to determine that the granulation unit constitutes a square MIMO system and that product quality can be tracked either by PSD average size (SGN_p) or spread (W_{2-4mm}). A Relative Gain Array study carried out for the granulation unit determined that the least interacting configuration is managed when the second chamber fluidized-bed level, the second chamber temperature and the top underpressure are controlled by manipulating the granulator product discharge, the fluidization air temperature and the fluidization air blower revolutions per minute, respectively. A sensitivity analysis allowed determining that the product SGN_p is the most appropriate variable to be controlled with the bottom crusher gap (GAP_L).

It was demonstrated that the temperature and underpressure loops present a very fast response, the fluidized-bed level control-loop performs reasonable, while the SGN_p time response results more sluggish. The servomechanism and regulatory tests performed by using a cascade control structure (specially designed to improve the product granulometry) outperform the single-loop control strategy for all the controlled variables.

This work provides valuable information to implement control strategies, commonly used in all large-scale plants that handle liquid and gases, to industrial granulation circuits that actually present none or very limited control loops. By the aid of the recently developed technologies for particle size in-line monitoring, granulation plant engineers can eliminate the typically observed product quality oscillations, as demonstrated through the implemented control strategies. Furthermore, the set-point tracking control performance shows that, if required, new market requirements of the granule mean size can be successfully achieved. The implemented control strategies are also useful in maintaining the desired plant nominal operation. In fact, it is demonstrated that typical plant upsets, such as variations in the plant feed or screen decks' fouling, can be rejected.

Table 7
Closed-loop set-point tracking performance parameters including a cascade controller.

Controller	ITAE
L_2	4.331E7 [m.s]
T_2	0.177 [K.s]
P_{top}	35.149 [Pa.s]
Master SGN_p	1.023E7 [s]

List of symbols

A_0^k	Passage area for granulator chamber k	[m^2]
Ap_T^k	Total particle superficial area for granulator chamber k	[m^2]
A_T^{damper}	Air duct cross-sectional area	[m^2]
A_T^{blower}	Blower duct cross-sectional area	[m^2]
$A_T^{scrubber}$	Scrubber cross-sectional area	[m^2]
A_T^k	Cross-sectional area for granulator chamber k	[m^2]
$bias_i$	Value of the manipulated variable for zero error	[Depends on the variable]
C_D	Discharge coefficient	[–]
Cp_a	Air mass heat capacity	[J/kg °C]
Cp_u	Solid urea mass heat capacity	[J/kg °C]
Cp_v	Water vapor mass heat capacity	[J/kg °C]
Cp_w	Liquid water mass heat capacity	[J/kg °C]
d	Particle diameter	[m]
e_i	Difference between the controlled variable and its set-point value	[Depends on the variable]
g	Gravity acceleration	[m/s^2]
$g_{i,j}$	Element of the transfer function matrix	[Depends on the variable]
$G(s)$	TFM, transfer function matrix	[–]
G_k	Growth rate for granulator chamber k	[m/s]
GAP_U	Distance between the crusher upper pair of rolls	[m]
GAP_L	Distance between the crusher lower pair of rolls	[m]
h_B	Screen bottom deck aperture	[m]
h_T	Screen top deck aperture	[m]
L_k	Fluidized-bed level for granulator chamber k	[m]
L_{weir}	Separating weir height	[m]
K	Gains matrix	[Depends on the variable]
$k_{i,j}$	Elements of the gain matrix	[Depends on the variable]
K_{c_i}	Controller gain	[Depends on the variable]
K_{damper}^k	Damper constant parameter for granulator chamber k	[–]
K_{grid}	Grid constant parameter	[–]
K_s	Scrubber constant parameter	[–]
$\dot{m}_a^k$	Fluidization air mass flowrate for granulator chamber k	[kg/s]
$\dot{m}_a^T$	Total fluidization air mass flowrate	[kg/s]
$\dot{m}_{in}^k$	Inlet mass flowrate for granulator chamber k	[kg/s]
$\dot{m}_{melt}^k$	Urea solution mass flowrate for granulator chamber k	[kg/s]
$\dot{m}_{out}^k$	Outlet mass flowrate for granulator chamber k	[kg/s]
m_T^k	Mass holdup for granulator chamber k	[kg]
$m_{T,0}^k$	Mass holdup for granulator chamber k at the initial steady state	[kg]
n^k	Number density function for granulator chamber k	[#/m]
n_0^k	Number density function for granulator chamber k at the initial steady state	[#/m]
$\dot{n}_{in}^k$	Inlet number flowrate expressed as density function for granulator chamber k	[#/m s]
$\dot{n}_{out}^k$	Outlet number flowrate expressed as density function for granulator chamber k	[#/m s]
$\dot{P}$	Product mass flowrate	[kg/s]
P_{top}	Granulator top underpressure	[Pa]
rpm	Air blower revolutions per minute	[rpm]
SGN_C	Milled stream size guide number	[mm.100]
SGN_P	Product stream size guide number	[mm.100]
t	Time	[s]
$T_{a,k}$	Fluidization air temperature for chamber k	[°C]
T_k	Temperature for granulator chamber k	[°C]
T_k^0	Temperature for granulator chamber k at the initial steady state	[°C]
T_{melt}^k	Urea solution temperature for granulator chamber k	[°C]
u_i	Manipulated variables	[Depends on the variable]
$\hat{u}_i$	Manipulated variables expressed as deviation variables	[Depends on the variable]
$U(s)$	Vector of manipulated variables	[Depends on the variable]
w	ITAE objective function weight factor	[–]
$W_{2-4\ mm}$	Mass fraction between 2 and 4 mm in the product stream	[%]
x_{melt}^k	Urea solution water mass fraction for granulator chamber k	[–]
y_i	Controlled variables	[Depends on the variable]
y_{SP_i}	Set-point of the controlled variables	[Depends on the variable]
$\hat{y}_i$	Controlled variables expressed as deviation variables	[Depends on the variable]
$Y(s)$	Vector of controlled variables	[Depends on the variable]

Greek symbols

α	Fraction of the granulator discharge area	[–]
Λ	RGA, relative gain array	[–]
$\lambda_{i,j}$	Elements of the RGA matrix	[–]
ΔH_{DIS}	Urea melt dissolution latent heat	[J/kg]
ΔH_{EV}	Water evaporation latent heat	[J/kg]
ΔP_{blower}	Energy supplied by the air blower	[Pa]
ΔP_{fan}	Energy supplied by the exhaust air fan	[Pa]
$\Delta P_{scrubber}$	Scrubber pressure drop	[Pa]
ε^k	Fluidized-bed porosity for granulator chamber k	[–]
$\varepsilon(s)$	Sensitivity function	[–]
$\eta(s)$	Complementary sensitivity function	[–]
ρ_a^k	Air density for granulator chamber k	[kg/m^3]
$\rho_{a,k}^{damper}$	Fluidization air density in the damper for granulator chamber k	[kg/m^3]
$\rho_{a,k}^{damper}$	Fluidization air density in the grid for granulator chamber k	[kg/m^3]
ρ_a^{in}	Fluidization air density in the blower suction	[kg/m^3]
ρ_a^{top}	Air density at the granulator top pressure and temperature	[kg/m^3]
ρ_{bed}^k	Fluidized-bed density for granulator chamber k	[kg/m^3]
ρ_p	Urea particle density	[kg/m^3]
τ_i	Controller integral time constant	[s]

Acknowledgments

The authors express their gratitude for the financial support by the Consejo Nacional de Investigaciones Científicas y Técnicas (CONICET) (PIP 2012-2014 112 201101 0033), Agencia Nacional de Promoción Científica y Tecnológica (ANPCyT) (PICT-2013-1765) and Universidad Nacional del Sur (UNS) of Argentina (PGI 24/M122).

Appendix A

This appendix briefly presents the equations of the fluidized-bed granulator model described in Section 2, based on Bertín et al. [54] and Cotabarren et al. [13]. The dynamic urea mass balance for chamber k is:

$$\frac{dm_T{}^k}{dt} = \dot{m}_{in}^k + \dot{m}_{melt}^k\left(1 - x_{melt}^k\right) - \dot{m}_{out}^k \qquad m_T^k(0) = m_{T,0}^k \tag{A.1}$$

where t represents the time, m_T^k, $\dot{m}_{in}^k$ and $\dot{m}_{out}^k$ are the solid mass holdup and inlet and outlet particle mass flowrates, respectively. $\dot{m}_{melt}^k$ and x_{melt}^k are the urea solution mass flowrate atomized into chamber k and its water mass fraction, respectively. According to Bertín et al. [52] it is accurate to assume that the urea solution water content evaporates immediately and completely; therefore the water mass balance can be neglected. The outlet solid mass flowrates are obtained by applying the Bernoulli equation:

$$\dot{m}_{out}^k = C_D A_0^k \sqrt{2g\rho_{bed}^k\left(\rho_{bed}{}^k L_k - \rho_{bed}^{k+1} L_{k+1}\right)} \qquad k = 1 \text{ to } 5 \tag{A.2}$$

$$\dot{m}_{out}^6 = C_D A_0^6 \rho_{bed}^6 \sqrt{2gL_k} \tag{A.3}$$

where A_0^k and L_k are the passage area and fluidized-bed height of chamber k, respectively. C_D is the discharge coefficient and ρ_{bed}^k is the bed density in compartment k as given by Bertín et al. [54].

To complete the set of equations, the fluidized-bed height within each chamber is computed as:

$$L_k = \frac{m_T^k}{\rho_{bed}^k A_T^k} \tag{A.4}$$

being A_T^k the cross-sectional area of chamber k.

The following dynamic energy balance given by Bertín et al. [54] is considered to compute the temperature T_k in each chamber:

$$\begin{aligned} & m_T^k Cp_u(T_k)\frac{dT_k}{dt} = \dot{m}_{in}^k \int_{T_k}^{T_{k-1}} Cp_u dT \\ & + \dot{m}_{melt}^k \left(1-x_{melt}^k\right) \int_{T_k}^{T_{melt}^k} Cp_u dT + \dot{m}_{melt}^k x_{melt}^k \int_{T_k}^{T_{melt}^k} Cp_w dT \\ & - \dot{m}_{melt}^k x_{melt}^k \Delta H_{EV}(T_k) + \dot{m}_{melt}^k \left(1-x_{melt}^k\right) \Delta H_{DIS}(T_{melt}) \\ & + \dot{m}_a^k \int_{T_k}^{T_a^k} Cp_a dT + \dot{m}_a^k Y_{a_{in}}^k \int_{T_k}^{T_a^k} Cp_v dT \qquad T_k(0) = T_k^0 \end{aligned} \tag{A.5}$$

where T_{melt}^k, T_a^k and T_{k-1} are the temperatures of the melt, fluidization air and solids entering the chamber k, respectively. T_k is the chamber temperature and, according to previous studies, can be accurately considered equal to the solid and air outlet temperatures [52]. For the granulator first chamber, T_{k-1} and $\dot{m}_{in}^k$ correspond to the seed temperature and mass flowrate, respectively. ΔH_{DIS} and ΔH_{EV} are the latent heats associated to the urea melt dissolution and water evaporation. Cp_u, Cp_w, Cp_a and Cp_v are the mass heat capacities of the solid urea, liquid water, air and water vapor, respectively. It is worth to mention that according to one of the model hypothesis, the gaseous and liquid phases operate at pseudo-steady state. Thus, the mass and energy accumulations of air and liquid within the fluidized chambers are neglected [52]. The energy balance complete derivation can be found elsewhere [68].

Bertín et al. [54] developed a population balance model for the urea fluidized-bed granulator assuming that only growth by coating occurs (elutriation, agglomeration, breakage, attrition and nucleation were supposed negligible). Thus, the dynamic population balance equation (PBE) for each well-mixed granulation chamber is given by:

$$\frac{\partial n^k}{\partial t} + \frac{\partial (G_k n^k)}{\partial d} = \dot{n}_{in}^k - \dot{n}_{out}^k \qquad IC: n^k(d,0) = n_0^k(d) \qquad BC: n^k(0,t) = 0 \tag{A.6}$$

being G_k the growth rate, d the particle diameter, $\dot{n}_{in}^k$ and $\dot{n}_{out}^k$ the number density function flows in and out of chamber k and $n_0^k(d)$ the number density function at the initial time, respectively. The PBE discretization technique developed by Hounslow et al. [16] and adopted by Bertín et al. [54] is implemented to solve the discretized form of Eq. (A.6).

Assuming that particles belonging to different size intervals grow proportional to its fractional surface area, G_k is defined as:

$$G_k = \frac{2\dot{m}_{melt}^k \left(1-x_{melt}^k\right)}{\rho_p A p_T^k} \tag{A.7}$$

where Ap_T^k denotes the total particle surface area within chamber k and ρ_p the particle density. This equation states that all the particles, independently of their sizes, grow at the same rate [1,2,54].

Finally, the momentum balance between the blower suction and the granulator top can be written as [13]:

$$\begin{aligned} & -\frac{0.5}{\rho_a^{in}}\left(\frac{\dot{m}_a^T}{A_T^{blower}}\right)^2 + \rho_a^k g L_k + P_{top} - P_{atm} - \Delta P_{blower} \\ & + \frac{K_{damper}^k}{\rho_{a,k}^{damper}}\left(\frac{\dot{m}_a^k}{A_T^{damper}}\right)^2 + \frac{K_{grid}}{\rho_{a,k}^{grid}}\left(\frac{\dot{m}_a^k}{A_T^k}\right)^2 + \left(\rho_p - \rho_a^k\right) g \left(1-\varepsilon^k\right) L_k = 0 \qquad k = 1..6 \end{aligned} \tag{A.8}$$

with:

$$P_{top} = P_{atm} + \Delta P_{scrubber} - \Delta P_{fan}. \tag{A.9}$$

The first term of Eq. (A.8) corresponds to the change in the kinetic energy between the blower suction and the granulator top, being ρ_a^{in} and A_T^{blower} the fluidization air density and the duct cross-sectional area at the blower suction, respectively; while $\dot{m}_a^T$ represents the total fluidization air flowrate (i.e., the sum of every chamber fluidization air flowrate, $\dot{m}_a^k$). As the granulator top cross-sectional area is considerably bigger than that of the blower suction duct, the air velocity at this point can be neglected. The second term represents the change in the potential energy, which only takes into account the contribution of the fluidized-bed height (L_k). Regarding the third term, atmospheric conditions are assumed at the blower suction while the top granulator pressure is determined by Eq. (A.9). ΔP_{blower} represents the energy supplied by the blower (that is determined through the manufacturer's performance curve) and depends on $\dot{m}_a^T$ and the blower operating revolutions per minute. The following term corresponds to the friction losses generated by the dampers; these are usually set at constant aperture, being the corresponding friction losses a function of the respective air mass flowrates, the air duct cross-sectional area (A_T^{damper}), the air density at the damper ($\rho_{a,k}^{damper}$) and a constant parameter that depends on the damper aperture (K_{damper}^k). The sixth term is related with the friction losses in the perforated plate (i.e., grid) and is proportional to the square velocity of the air that passes through it. K_{grid} is a constant that depends on the design and geometry of the perforated plate [2]. For chamber k, A_T^k represents the cross-sectional area and $\rho_{a,k}^{grid}$ the air density at the grid entrance. The last term accounts for the friction pressure drop in each fluidized-bed, which is a result of the force balance between the particles and the fluid [2], being ρ_a^k the air density and ε^k the porosity corresponding to chamber k. The values for the damper (K_{damper}^k) and grid (K_{grid}) constants can be found elsewhere [68]. Eq. (A.9) represents a simplified momentum balance between the granulator top and the atmospheric discharge (potential and kinetic energy terms have been neglected). For the sake of simplicity and to guarantee the desired underpressure at the granulator top, both $\Delta P_{scrubber}$ and ΔP_{fan} have been represented as proportional to the fluidization air flowrate:

$$\Delta P_{scrubber} - \Delta P_{fan} = -\frac{K_s}{\rho_a^{top}}\left(\frac{\dot{m}_a^T}{A_T^{scrubber}}\right)^2 \tag{A.10}$$

where

K_s is a proportional constant determined for the nominal operation values, $A_T^{scrubber}$ is the scrubber cross-sectional area and ρ_a^{top} is the air density at the granulator top pressure and temperature. This last balance can be refined if both units (scrubber and exhaust fans) are described by individual models and the kinetic and potential energy terms are included. Nevertheless, Eq. (A.10) is appropriate to fulfill the objectives of this contribution.

References

[1] J.D. Litster, B.J. Ennis, L. Liu, The Science and Engineering of Granulation Processes, Particle Technology Series, Kluwer Academic Publishers, Dordrecht, 2004.
[2] L. Mörl, S. Heinrich, M. Peglow, Fluidized bed spray granulation, in: A.D. Salman, M.J. Hounslow, J.P.K. Seville (Eds.), Handb. Powder Technol. Elsevier, Amsterdam, The Netherlands, 2007.

[3] M. Peglow, J. Kumar, S. Heinrich, G. Warnecke, E. Tsotsas, L. Morl, et al., A generic population balance model for simultaneous agglomeration and drying in fluidized beds, Chem. Eng. Sci. 62 (2007) 513–532, http://dx.doi.org/10.1016/j.ces.2006.09.042.

[4] A. Burggraeve, T. Monteyne, C. Vervaet, J.P. Remon, T. De Beer, Process analytical tools for monitoring, understanding, and control of pharmaceutical fluidized bed granulation: a review, Eur. J. Pharm. Biopharm. 83 (2013) 2–15, http://dx.doi.org/10.1016/j.ejpb.2012.09.008.

[5] K. Saleh, P. Guigon, Coating and encapsulation processes in powder technology, in: A.D. Salman, M.J. Hounslow, J.P.K. Seville (Eds.), Handb. Powder Technol. Elsevier, Amsterdam, The Netherlands, 2007.

[6] H. Zhai, S. Li, D.S. Jones, G.M. Walker, G. Andrews, The effect of the binder size and viscosity on agglomerate growth in fluidised hot melt granulation, Chem. Eng. J. 164 (2010) 275–284, http://dx.doi.org/10.1016/j.cej.2010.08.056.

[7] I.M. Cotabarren, D. Bertín, S. Veliz, L. Mirazú, J. Piña, V. Bucalá, Production of granular urea as nitrogenous fertilizer, in: C.M. Muñoz, A.M. Fernández (Eds.), Urea Synth. Prop. Uses, NOVA Publishers 2012, pp. 1–63.

[8] N. Balliu, An Object Oriented Approach to the Modelling and Dynamics of Granulation Circuits, 2005.

[9] D. Bertín, I. Cotabarren, J. Piña, V. Bucalá, Granule size distribution for a multichamber fluidized-bed melt granulator: modeling and validation using process measurement data, Chem. Eng. Sci. 104 (2013) 319–329, http://dx.doi.org/10.1016/j.ces.2013.08.012.

[10] R. Ramachandran, A. Chaudhury, Model-based design and control of a continuous drum granulation process, Chem. Eng. Res. Des. 90 (2012) 1063–1073, http://dx.doi.org/10.1016/j.cherd.2011.10.022.

[11] C. Reimers, J. Werther, G. Gruhn, Design specifications in the flowsheet simulation of complex solids processes, Powder Technol. 191 (2009) 260–271, http://dx.doi.org/10.1016/j.powtec.2008.10.012.

[12] J. Werther, S. Heinrich, M. Dosta, E.-U. Hartge, The ultimate goal of modeling—simulation of system and plant performance, Particuology 9 (2011) 320–329, http://dx.doi.org/10.1016/j.partic.2011.03.006.

[13] I. Cotabarren, D. Bertín, V. Bucalá, J. Piña, A validated flowsheeting tool for the study of an industrial granulation process, Ind. Eng. Chem. Res. 52 (2013) 15198–15210.

[14] H.M. Hulburt, S. Katz, Some problems in particle technology, Chem. Eng. Sci. 19 (1964) 555–574, http://dx.doi.org/10.1016/0009-2509(64)85047-8.

[15] A.D. Randolph, M.A. Larson, Theory of Particulate Processes, Academic Press, New York, United States, 1971.

[16] M.J. Hounslow, R. Ryall, V.R. Marshall, A discretized population balance for nucleation, growth, and aggregation, AIChE J. 34 (1988) 1821–1832.

[17] D. Ramkrishna, Population Balances, Academic Press, London, England, 2000.

[18] J. Li, B. Freireich, C. Wassgren, J.D. Litster, A general compartment-based population balance model for particle coating and layered granulation, AIChE J. 58 (2012) 1397–1408.

[19] M. Dueñas Diez, B. Erikydstie, M. Fjeld, B. Lie, Inventory control of particulate processes, Comput. Chem. Eng. 32 (2008) 46–67, http://dx.doi.org/10.1016/j.compchemeng.2007.01.007.

[20] A. Bück, S. Palis, E. Tsotsas, Model-based control of particle properties in fluidised bed spray granulation, Powder Technol. (2014)http://dx.doi.org/10.1016/j.powtec.2014.07.023.

[21] F. Boukouvala, V. Niotis, R. Ramachandran, F.J. Muzzio, M.G. Ierapetritou, An integrated approach for dynamic flowsheet modeling and sensitivity analysis of a continuous tablet manufacturing process, Comput. Chem. Eng. 42 (2012) 30–47, http://dx.doi.org/10.1016/j.compchemeng.2012.02.015.

[22] T. Chiu, P.D. Christofides, Nonlinear control of particulate processes, 45 (1999) 1279–1297.

[23] T.Y. Chiu, P.D. Christofides, Robust control of particulate processes using uncertain population balances, AIChE J. 46 (2000) 266–280, http://dx.doi.org/10.1002/aic.690460207.

[24] N.H. El-Farra, T.Y. Chiu, P.D. Christofides, Analysis and control of particulate processes with input constraints, AIChE J. 47 (2001) 1849–1865, http://dx.doi.org/10.1002/aic.690470815.

[25] A. Kalani, P.D. Christofides, Nonlinear control of spatially inhomogenous aerosol processes, Chem. Eng. Sci. 54 (1999) 2669–2678, http://dx.doi.org/10.1016/S0009-2509(98)00315-7.

[26] A. Kalani, P.D. Christofides, Simulation, estimation and control of size distribution in aerosol processes with simultaneous reaction, nucleation, condensation and coagulation, Comput. Chem. Eng. 26 (2002) 1153–1169, http://dx.doi.org/10.1016/S0098-1354(02)00032-7.

[27] D. Shi, P. Mhaskar, N.H. El-Farra, P.D. Christofides, Predictive control of crystal size distribution in protein crystallization, Nanotechnology 16 (2005) S562–S574, http://dx.doi.org/10.1088/0957-4484/16/7/034.

[28] D. Shi, N.H. El-Farra, M. Li, P. Mhaskar, P.D. Christofides, Predictive control of particle size distribution in particulate processes, Chem. Eng. Sci. 61 (2006) 268–281, http://dx.doi.org/10.1016/j.ces.2004.12.059.

[29] P.D. Christofides, N.H. El-Farra, M. Li, P. Mhaskar, Model-based control of particulate processes, Chem. Eng. Sci. 63 (2008) 1156–1172, http://dx.doi.org/10.1016/j.ces.2007.07.017.

[30] J. Zhang, J.D. Litster, F.Y. Wang, I.T. Cameron, Evaluation of control strategies for fertiliser granulation circuits using dynamic simulation, Powder Technol. 108 (2000) 122–129, http://dx.doi.org/10.1016/S0032-5910(99)00209-0.

[31] M. Pottmann, B.A.A. Ogunnaike, A.A. Adetayo, B.J. Ennis, Model-based control of a granulation system, Powder Technol. 108 (2000) 192–201, http://dx.doi.org/10.1016/S0032-5910(99)00220-X.

[32] E. Gatzke, F.J. Doyle III, Model predictive control of a granulation system using soft output constraints and prioritized control objectives, Powder Technol. 121 (2001) 149–158, http://dx.doi.org/10.1016/S0032-5910(01)00334-5.

[33] C.F.W. Sanders, M.J. Hounslow, F.J. Doyle III, Identification of models for control of wet granulation, Powder Technol. 188 (2009) 255–263, http://dx.doi.org/10.1016/j.powtec.2008.05.005.

[34] T. Glaser, C.F.W. Sanders, F.Y. Wang, I.T. Cameron, J.D. Litster, J.M.-H. Poon, et al., Model predictive control of continuous drum granulation, J. Process Control 19 (2009) 615–622, http://dx.doi.org/10.1016/j.jprocont.2008.09.001.

[35] S. Heinrich, M. Peglow, M. Ihlow, M. Henneberg, L. Morl, Analysis of the start-up process in continuous fluidized bed spray granulation by population balance modelling, Chem. Eng. Sci. 57 (2002) 4369–4390, http://dx.doi.org/10.1016/S0009-2509(02)00352-4.

[36] S. Heinrich, M. Peglow, M. Ihlow, L. Morl, Particle population modeling in fluidized bed-spray granulation—analysis of the steady state and unsteady behavior, Powder Technol. 130 (2003) 154–161, http://dx.doi.org/10.1016/S0032-5910(02)00259-0.

[37] J. Drechsler, M. Peglow, S. Heinrich, M. Ihlow, L. Morl, Investigating the dynamic behaviour of fluidized bed spray granulation processes applying numerical simulation tools, Chem. Eng. Sci. 60 (2005) 3817–3833, http://dx.doi.org/10.1016/j.ces.2005.02.010.

[38] R. Radichkov, T. Muller, A. Kienle, S. Heinrich, M. Peglow, L. Morl, A numerical bifurcation analysis of continuous fluidized bed spray granulation with external product classification, Chem. Eng. Process. 45 (2006) 826–837, http://dx.doi.org/10.1016/j.cep.2006.02.003.

[39] S. Palis, A. Kienle, Stabilization of continuous fluidized bed spray granulation with external product classification, Chem. Eng. Sci. 70 (2012) 200–209, http://dx.doi.org/10.1016/j.ces.2011.08.026.

[40] S. Palis, A. Kienle, H_∞ loop shaping control for continuous fluidized bed spray granulation with internal product classification, Ind. Eng. Chem. Res. 52 (2013) 408–420.

[41] S. Palis, A. Kienle, Discrepancy based control of particulate processes, J. Process Control 24 (2014) 33–46, http://dx.doi.org/10.1016/j.jprocont.2013.12.003.

[42] R. Ramachandran, J. Arjunan, A. Chaudhury, M.G. Ierapetritou, Model-based control-loop performance of a continuous direct compaction process, J. Pharm. Innov. 6 (2011) 249–263, http://dx.doi.org/10.1007/s12247-011-9118-2.

[43] R. Singh, M. Ierapetritou, R. Ramachandran, An engineering study on the enhanced control and operation of continuous manufacturing of pharmaceutical tablets via roller compaction, Int. J. Pharm. 438 (2012) 307–326, http://dx.doi.org/10.1016/j.ijpharm.2012.09.009.

[44] R. Singh, D. Barrasso, A. Chaudhury, M. Sen, M. Ierapetritou, R. Ramachandran, Closed-loop feedback control of a continuous pharmaceutical tablet manufacturing process via wet granulation, J. Pharm. Innov. (2014) http://dx.doi.org/10.1007/s12247-014-9170-9.

[45] R. Singh, M. Ierapetritou, R. Ramachandran, System-wide hybrid MPC–PID control of a continuous pharmaceutical tablet manufacturing process via direct compaction, Eur. J. Pharm. Biopharm. 85 (2013) 1164–1182.

[46] P. Heffer, M. Prud'homme, Fertilizer outlook 2014–2018, 82nd IFA Annu. Conf., Sydney, Australia 2014, pp. 26–28.

[47] A. Niks, W. Van Hijfte, R. Goethals, Process for Urea Granulation, 1980.

[48] A. Kayaert, R. Antonus, Process for the Production of Urea Granules, 1997. 5653781.

[49] M. Halstensen, P. Debakker, K. Esbensen, Acoustic chemometric monitoring of an industrial granulation production process—a PAT feasibility study, Chemom. Intell. Lab. Syst. 84 (2006) 88–97, http://dx.doi.org/10.1016/j.chemolab.2006.05.012.

[50] A. Alnajar, Framing the best practices in granulation operation, Arab. Fertil. 58 (2010) 26–29.

[51] A. Kayaert, N.S.M. fluidised-bed urea granulation process, Proc. 30th Annu. Meet. Fertil. Ind. Round Table, 1980.

[52] D. Bertín, G. Mazza, J. Piña, V. Bucalá, Modeling of an industrial fluidized-bed granulator for urea production, Ind. Eng. Chem. Res. 46 (2007) 7667–7676, http://dx.doi.org/10.1021/ie070361o.

[53] I.M. Cotabarren, D. Bertín, J. Piña, V. Bucalá, Analysis of optimal control problems and plant debottlenecking for urea granulation circuits, Ind. Eng. Chem. Res. 50 (2011) 11996–12010.

[54] D. Bertín, I.M. Cotabarren, V. Bucalá, J. Piña, Analysis of the product granulometry, temperature and mass flow of an industrial multichamber fluidized bed urea granulator, Powder Technol. 206 (2011) 122–131, http://dx.doi.org/10.1016/j.powtec.2010.06.016.

[55] D. Bertín, Modelado y Simulación de un Granulador de Lecho Fluidizado para la Producción de Urea, Universidad Nacional del Sur, Argentina, 2011.

[56] I.M. Cotabarren, J. Rossit, V. Bucala, J. Piña, Modeling of an industrial vibrating double-deck screen of a urea granulation circuit, Ind. Eng. Chem. Res. 48 (2009) 3187–3196, http://dx.doi.org/10.1021/ie800968y.

[57] I.M. Cotabarren, P.G. Schulz, V. Bucalá, J. Piña, Modeling of an industrial double-roll crusher of a urea granulation circuit, Powder Technol. 183 (2008) 224–230, http://dx.doi.org/10.1016/j.powtec.2007.07.023.

[58] Process System Enterprise, gPROMS, 2014.

[59] S.M. Nowee, A. Abbas, J. Romagnoli, Model-based optimal strategies for controlling particle size in antisolvent crystallization operations, Cryst. Growth Des. 8 (2008) 2698–2706, http://dx.doi.org/10.1021/cg700720t.

[60] I.M. Cotabarren, V. Bucalá, J. Piña, Desarrollo de un simulador tipo flowsheet para circuitos de granulación de fertilizantes y su aplicación a estudios de control, 3rd Argentine Symp. Ind. Informatics — 43 JAIIO, SADIO, Buenos Aires, Argentina, 2014.

[61] J. Romagnoli, A. Palazoglu, Introduction to Process Control, Taylor & Francis, Boca Raton, FL, 2006.
[62] Karnaphuli Fertilizer Company Limited. Rangadia, Anowara Chittagong, Bangladesh, 2014.
[63] I.M. Cotabarren, D. Bertín, J. Romagnoli, V. Bucalá, J. Piña, Dynamic simulation and optimization of a urea granulation circuit, Ind. Eng. Chem. Res. 49 (2010) 6630–6640, http://dx.doi.org/10.1021/ie901885x.
[64] S. Watano, Direct control of wet granulation processes by image processing system, Powder Technol. 117 (2001) 163–172, http://dx.doi.org/10.1016/S0032-5910(01)00322-9.
[65] S. Watano, T. Numa, K. Miyanami, Y. Osako, A fuzzy control system of high shear granulation using image processing, Powder Technol. 115 (2001) 124–130, http://dx.doi.org/10.1016/S0032-5910(00)00332-6.
[66] M. Sen, R. Singh, R. Ramachandran, Simulation-based design of an efficient control system for the continuous purification and processing of active pharmaceutical ingredients, J. Pharm. Innov. (2014) http://dx.doi.org/10.1007/s12247-014-9173-6.
[67] D.E. Seborg, T.F. Edgar, D.A. Mellichamp, Process Dynamics and Control, 2nd ed. John Wiley & Sons, Inc., 2004
[68] I.M. Cotabarren, Modelado y Simulación del Sector de Granulación de una Planta de Urea, Universidad Nacional del Sur, Argentina, 2012..